

Cite this: *Chem. Soc. Rev.*, 2012, **41**, 3679–3698

www.rsc.org/csr

## CRITICAL REVIEW

## Functionalized mesoporous silica materials for controlled drug delivery

Piaoping Yang,<sup>ab</sup> Shili Gai<sup>b</sup> and Jun Lin<sup>\*a</sup>

Received 11th November 2011

DOI: 10.1039/c2cs15308d

In the past decade, non-invasive and biocompatible mesoporous silica materials as efficient drug delivery systems have attracted special attention. Great progress in structure control and functionalization (magnetism and luminescence) design has been achieved for biotechnological and biomedical applications. This review highlights the most recent research progress on silica-based controlled drug delivery systems, including: (i) pure mesoporous silica sustained-release systems, (ii) magnetism and/or luminescence functionalized mesoporous silica systems which integrate targeting and tracking abilities of drug molecules, and (iii) stimuli-responsive controlled release systems which are able to respond to environmental changes, such as pH, redox potential, temperature, photoirradiation, and biomolecules. Although encouraging and potential developments have been achieved, design and mass production of novel multifunctional carriers, some practical biological application, such as biodistribution, the acute and chronic toxicities, long-term stability, circulation properties and targeting efficacy *in vivo* are still challenging.

## 1. Introduction

Encouraged by the exciting discovery of the new family of molecular sieves generically called M41S in the early 1990s,<sup>1</sup> research on mesoporous silica materials has received burgeoning attention, and advanced rapidly. The most well known and common mesoporous silica materials include MCM-41, MCM-48 and SBA-15, which present different pore sizes (2 to 10 nm) and structural characteristics (2D hexagonal and 3D cubic).

The mesoporous silica materials are synthesized in the presence of assembled cationic surfactant micelle templates, which serve as structure-directing agents for polymerizing silica component by electrostatic interaction, as illustrated in Fig. 1. The controllable synthesis protocol, outstanding mesoporous structure and surface with silanol groups make mesoporous silica materials have unique properties, such as large surface area, high pore volume, uniform and tunable pore size (easily realized by varying the surfactants), low mass density, non-toxic nature, easily modified surface properties, and good biocompatibility.<sup>2–7</sup> Therefore, ordered mesoporous materials have been shown to be important candidates in sensors, catalysts, biomedicine and even in environmental applications.<sup>8–11</sup>

In 2001, a MCM-41-type mesoporous silica material was first reported as a drug delivery system.<sup>12</sup> Drug delivery

<sup>a</sup> State Key Laboratory of Rare Earth Resource Utilization, Changchun Institute of Applied Chemistry, Chinese Academy of Sciences, Changchun, 130022, P. R. China. E-mail: jlin@ciac.jl.cn

<sup>b</sup> Key Laboratory of Superlight Materials and Surface Technology, Ministry of Education, Harbin Engineering University, Harbin, 150001, P. R. China



Piaoping Yang

Piaoping Yang is currently a Professor of chemistry in the Department of College of Material Science and Chemical Engineering at Harbin Engineering University. He received his Bachelor of Science degree at Nankai University and his PhD degree at Jilin University. After graduation he joined Prof. Jun Lin's group for postdoctoral research. His research mainly focuses on the fabrication and biomedical applications of rare earth based functional materials.



Shili Gai

Shili Gai was born in Jilin, China in 1986. She received her BS degree from Harbin Engineering University, China in 2005. She is currently pursuing her PhD under the supervision of Prof. Piaoping Yang at Harbin Engineering University. Her research focuses on the functional mesoporous silica materials used for drug delivery, including the study of the physical chemical properties and the biomedical applications of these materials.

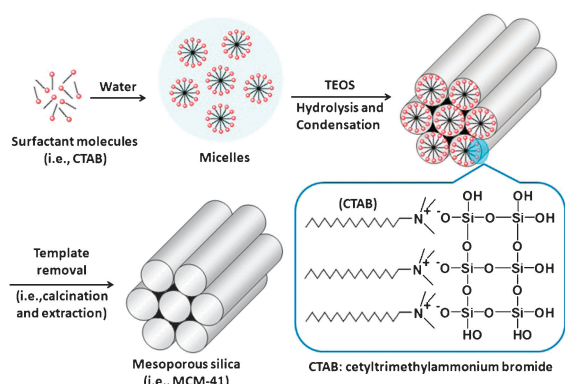


**Fig. 1** Scheme of the formation mechanism of MCM-41.

systems, which can deliver precise quantities of therapeutic drugs to the targeted cells or tissues in a tailored release manner to enhance drug efficiency and reduce toxicity,<sup>13,14</sup> have been one of the most promising applications for human health care and represent an ever-evolving field for biomedical materials science.<sup>15–18</sup> In recent years, mesoporous silica materials have been considered to be excellent candidates as carriers for drug delivery. On the one hand, textural properties of mesoporous silica increase the loading amount of drugs by hosting them within pore channels. On the other hand, the silanol-containing surface can be easily functionalized, allowing for a better control over the drug diffusion kinetics.<sup>19,20</sup> In addition, multifunctional mesoporous silica composites with excellent magnetic and/or luminescent properties represent another grand challenge for drug delivery targeting and tracking. Luminescent materials (such as organic dyes, quantum dots, and rare-earth nanophosphors) or magnetic nanoparticles have been successfully used to functionalize the mesoporous silica in the form of core-shell, embedded and rattle-type structures. The rapid development of novel luminescent and magnetic nanomaterials will lead to the enrichment of multifunctional mesoporous silica composites with improved properties.



**Jun Lin**

*Jun Lin was born in Changchun, China, in 1966. He received BS and MS degrees in inorganic chemistry from Jilin University, China in 1989 and 1992, respectively, and a PhD degree (inorganic chemistry) from the Changchun Institute of Applied Chemistry in 1995. Then he went to City University of Hong Kong (1996), Institute of New Materials (Germany, 1997), Virginia Commonwealth University (USA, 1998) and University of New Orleans (USA, 1999) working as a*

*postdoctor. He came back to China in 2000, and since then has been working as a professor in CIAC. His research interests include bulk and nanostructured luminescent materials and multifunctional composite materials together with their applications in display, lightening and biomedical fields.*

Therefore, innovative research is ongoing on silica-based drug delivery systems, including structure design and functional optimization.<sup>21</sup> Meanwhile, the biosafety research on mesoporous silica materials at different levels from molecule, cell, blood to tissue, involving blood compatibility,<sup>22–25</sup> cytotoxicity,<sup>26,27</sup> biodegradability,<sup>28–30</sup> biodistribution and excretion,<sup>31–34</sup> also becomes a hot topic and receives satisfied results.

Clearly, we cannot exhaustively cover the whole field, so our efforts here are to highlight the recent studies on mesoporous silica sustained drug delivery systems (SDDSs) and stimuli-responsive controlled drug delivery systems (CDDSs) classified by a drug delivery mechanism. Sustained drug delivery is aroused by the molecular diffusion of adsorbed drugs, from their carriers toward the surrounding media, depending exclusively on a concentration gradient. Thus the release occurred immediately when the carrier is introduced into the media, which is suitable for accumulating a drug at a targeted site. Controlled drug delivery offers triggered release of therapeutic drugs by using a chemical/physical response of the carriers to an environmental/external stimulus, which can start the drug release on demand. To date, many model drugs, such as pharmaceutical drugs, proteins, and imaging dyes have been studied for adsorption and release in drug delivery systems (Table 1). Pharmaceutical drugs have been used in both SDDSs and CDDSs to study the drug release efficiency. Dye is another widely used model drug due to the characteristic and monitored fluorescent properties, especially in CDDSs. However, due to the small pore sizes of the MCM-type materials, larger molecules such as proteins and enzymes have been used rarely.

This review first provides a brief summary of the influence of textural properties (pore size, structure, morphology, and surface properties) on drug loading and release properties. The novel hollow mesoporous silica drug delivery systems with a high surface area and large pore volume which enable a high drug loading amount are described in this part. Secondly, we highlight the recent research progress on multifunctional mesoporous silica SDDSs with the abilities to target and track drug molecules by the integrating luminescence and magnetism. Finally, we review the smart stimuli-responsive CDDSs that can respond to external stimuli, such as pH, redox potential, temperature, photoirradiation, and biomolecules.

## 2. Pure mesoporous silica SDDSs

### 2.1. Conventional mesoporous silica SDDSs

The early mesoporous silica SDDSs were mainly based upon the physical and textural properties of the conventional mesoporous silica materials such as MCM-41, MCM-48 and SBA-15 with empty mesopore channels (Fig. 1) to absorb/encapsulate relatively large amounts of bioactive molecules. The groups of Vallet-Regí and Lindén have systematically studied the influence of pore diameter, pore structure, surface area, and pore volume on drug loading amount and release rate.<sup>60</sup> We summarize the results as following:

#### (i) Pore diameter

The decrease in pore diameter leads to a decrease in drug loading amount and release rate, which can be linked to a steric hindrance effect. This effect was observed when the pore

**Table 1** Pharmacology, adsorption and release mechanism of different model drugs

Model drug	Pharmacology	Carrier	Adsorption mechanism	Release mechanism	Ref.
Doxorubicin	Anticancer drug	1. Rattle-type Fe <sub>3</sub> O <sub>4</sub> @mSiO <sub>2</sub>	Electrostatic interaction	Dissolution-diffusion controlled mechanism	35
Camptothecin	Anticancer drug	2. β-CD capped MSNs	Electrostatic interaction	pH responsive release	36
		1. Fe <sub>3</sub> O <sub>4</sub> and dye functionalized MSNs	Simple impregnation	Diffusion controlled mechanism	37
Paclitaxel	Anticancer drug	2. Fe <sub>3</sub> O <sub>4</sub> NPs capped MSNs	Simple impregnation	Magnetic field responsive release	38
		1. Fe <sub>3</sub> O <sub>4</sub> and dye functionalized MSNs	Simple impregnation	Diffusion controlled mechanism	37
Irinotecan hydrochloride trihydrate	Anticancer drug	2. Au NPs capped MCM-41	Simple impregnation	Photo responsive release	39
		Double shelled hollow mesoporous silica spheres	Simple impregnation	Diffusion controlled mechanism	40
Docetaxel	Anticancer drug	Rattle-type Fe <sub>3</sub> O <sub>4</sub> @mSiO <sub>2</sub>	Simple impregnation	Diffusion controlled mechanism	41
Ibuprofen	Anti-inflammatory/analgesic	1. Fe <sub>3</sub> O <sub>4</sub> functionalized SBA-15	Physical adsorption and hydrogen bond	Diffusion controlled mechanism	42
		2. Hollow MSNs capped with PAH/PSS multilayers	Simple impregnation	pH responsive release	43
Aspirin	Anti-inflammatory/analgesic	Rattle-type Fe <sub>3</sub> O <sub>4</sub> @mSiO <sub>2</sub>	Physical adsorption and hydrogen bond	Fickian diffusion mechanism	44
Dexamethasone	Anti-inflammatory	Fe <sub>3</sub> O <sub>4</sub> NPs capped MSNs	Impregnation	pH responsive release	45
Captopril	Anti-hypertensive	MSNs/apatite composite	Physical adsorption and hydrogen bond	Diffusion controlled mechanism	46
Gentamycin	Antibiotic	Hollow MSNs capped with PAH/PSS multilayers	Simple impregnation	pH responsive release	47
Erythromycin	Antibiotic	Hydrophobic group modified SBA-15	Impregnation	Diffusion controlled mechanism	48
Vancomycin	Antibiotic	CdS NPs capped MCM-41	Impregnation	Reducing agents responsive release	7
Alendronate	Anti-psoriatic	Propylamine groups modified MCM-41 and SBA-15	Electrostatic attraction	Diffusion controlled mechanism	49
ZnPcS <sub>4</sub>	Photodynamic therapy drug	Polymer shell capped MSNs	Impregnation	Thermo responsive release	50
Salvianolic acid B	Blood-circulation accelerating agent and antioxidant	Dye grafted SBA-15	Electrostatic attraction	Diffusion controlled mechanism	25
Fluorescein (dye)	—	DNA capped MSNs	Simple impregnation	Diffusion controlled mechanism	51
Rhodamine B (dye)	—	α-CD capped MSNs	Simple impregnation	Enzyme responsive release	52
[Ru(bipy) <sub>3</sub> ] <sup>2+</sup> (dye)	—	Polyamine capped MSNs	Simple impregnation	pH and anion responsive release	53
Propidium Iodide (dye)	—	CB[6] capped MSNs	Post synthesis grafting	pH responsive release	54
Hoechst 33342 (dye)	—	α-CD capped hollow MSNs	Simple impregnation	pH responsive release	55
Calcein (dye)	—	CB[7] capped MCM-41	Simple impregnation	pH and competitor responsive release	56
Coumarin 540A (dye)	—	Azobenzene derivatives functionalized MSNs	Co-condensation	Photo responsive release	57
Safranin O (dye)	—	Au NPs capped MSNs	Simple impregnation	Photo and pH responsive	58
Lysozyme (Enzyme)	—	CaWO <sub>4</sub> :Tb <sup>3+</sup> functionalized SBA-15	Electrostatic interaction	Diffusion controlled mechanism	59
Bovine Serum Albumin (Enzyme)	—	SBA-15	Simple impregnation	Diffusion controlled mechanism	60
Cysteine (Amino acid)	—	Mercapto group functionalized MSNs	Chemically attached <i>via</i> thioether bonds	Cell responsive release	61
Vitamine-B <sub>2</sub> (Nutriment)	—	Polyamines capped MCM-41	Simple impregnation	pH and anion responsive release	62
Insulin	—	Enzyme multilayers capped MSNs	Simple impregnation	Glucose responsive release	63
Adenosine triphosphate	—	CdS NPs capped MCM-41	Simple impregnation	Reducing agents responsive release	7

MSNs: mesoporous silica nanoparticles; mSiO<sub>2</sub>: mesoporous silica layer; NPs: nanoparticles; ZnPcS<sub>4</sub>: Zn(II) phthalocyanine tetrasulfonic acid; CB[6], α-CD, CB[7], β-CD: macrocyclic organic molecules (detail in part 4).

diameters of SBA-15 differ from 8.2 to 11.4 nm resulting in the increase of bovine serum albumin loading from 15% up to 27%.<sup>60</sup> In addition, the decrease in pore diameter of MCM-41 or MCM-48 leads to a decrease in the release rate of ibuprofen (IBU), erythromycin and other drugs, which is depicted in Fig. 2.<sup>64,65</sup> Qu *et al.* pointed out that the pore-size

effect can be evaluated only if the morphology is similar at the microstructure level.<sup>66</sup>

#### (ii) Pore structure types

Structure types, in terms of pore connectivity and geometry, seem to have an influence on the drug loading and release properties. It is true that the interconnected pore systems



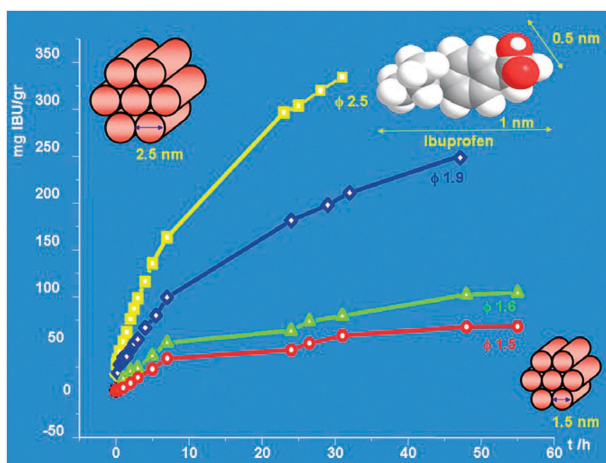


**Fig. 2** Release patterns of adsorbed ibuprofen in MCM-41 matrices with four different pore sizes. (Adapted from ref. 18, Copyright 2006, Wiley-VCH Verlag GmbH & Co. KGaA. Reproduced with permission.).

provide easier and faster diffusion process than unconnected pore systems, but, the effect is weak. Lindén *et al.* demonstrated that a type of SBA-1 material with 3D cubic interconnected pores shows a slightly faster IBU release rate and similar drug loading amount when compared with another type of SBA-3 with similar pore diameter and surface area, while having unconnected pores.<sup>67</sup> Another example, by comparing both kinetic constants of MCM-41 with a 2D hexagonal arrangement and MCM-48 with a 3D cubic pore system, a slightly faster release rate of IBU is observed for the 3D-pore system by Vallet-Regí *et al.*<sup>68</sup> In addition, Lindén *et al.* also indicated that a one-dimensional pore structure with cage-like pores is the most promising pore geometry for providing a high drug loading amount and slow drug release rate by comparing it with other types of pore structures.<sup>67</sup>

### (iii) Surface area

The specific surface area is an important factor governing the amount of retained drug molecules, usually hydrophilic or possessing functional groups, due to the chemically or physically adsorptive property of Si–OH groups in drug-loading process. A high surface area with more Si–OH groups will provide more active sites, resulting in an increased drug loading amount. For example, the maximum amount of alendronate loaded into MCM-41 ( $1157 \text{ m}^2 \text{ g}^{-1}$ ) and SBA-15 ( $719 \text{ m}^2 \text{ g}^{-1}$ ) matrices are 14% and 8%, respectively.<sup>49,68</sup> They also proved that surface areas and mesopore sizes would have combined effects on the release kinetics: alendronate released from the above MCM-41 (3 nm) exhibits first order kinetics, whereas release from SBA-15 (9 nm) shows linear or zero order kinetics.

### (iv) Pore volume

The pore volume is another important, even ruling factor influencing the drug loading, which can be described as the larger the pore volume the higher the drug loading amount. For instance, the loading amount of bovine serum albumin in SBA-15 ( $1.1 \text{ cm}^3 \text{ g}^{-1}$ ) and mesocellular silica foams ( $1.9 \text{ cm}^3 \text{ g}^{-1}$ ) is 15% and 24%, respectively.<sup>60,69</sup>

### (v) Surface functionalization

Typically, drug molecules are loaded in mesoporous silica carriers through weak non-covalent interactions, such as hydrogen bonding, physical adsorption, electrostatic interaction, and  $\pi$ - $\pi$  stacking.<sup>70</sup> Thereby, chemical modification of the carrier

with appropriate functional groups, presenting attractive interactions with biologically active molecules, may provide an effective control on the drug adsorption amount and sustained release rate.<sup>18,49,71</sup> The pioneering case of surface functionalization is IBU adsorbed into MCM-41 modified with amine groups. Without modification, the hydrogen bond takes place between the silanol group of the matrix and the carboxylic acid group from the drug. Whereas, after modification, a much stronger electrostatic attracting interaction between the carboxylic acid and amine group (modified MCM-41) leads to the increase in the drug loading and a slower IBU release rate.<sup>18</sup> Another example, the loading of tryptophan in SBA-15 and SBA-15 modified with quaternary alkyl amines, provides the same conclusion as above.<sup>72</sup>

## 2.2. Improved hollow mesoporous silica SDDSs

Recently, hollow mesoporous silica (HMS) materials, which simultaneously possess large voids inside the shells and mesopores at the shells, have attracted widespread attention. The large voids can store more drug molecules than that of the conventional mesoporous silica materials. The ordered mesopores at the shells, on the one hand, can provide accessible channels for drug molecules diffusion and mass transfer without blocking; on the other hand, could control the permeability of the shells for matter exchange between voids and the outer environment. This conclusion is not just a logical hypothesis. Shi *et al.* have proved that the maximum IBU storage capacity of a hollow structure ( $302 \text{ mg g}^{-1}$ ) is not much lower than the reported maximum IBU storage capacity of MCM-41 ( $358 \text{ mg g}^{-1}$ ), although the surface area and pore volume of the hollow structure ( $436 \text{ m}^2 \text{ g}^{-1}$ ,  $0.53 \text{ cm}^3 \text{ g}^{-1}$ ) are much lower than those of MCM-41 ( $1152 \text{ m}^2 \text{ g}^{-1}$ ,  $0.99 \text{ cm}^3 \text{ g}^{-1}$ ).<sup>73</sup> This is because in conventional mesoporous materials, effective pore volume would decrease rapidly once the drug molecules are adsorbed as a result of blocking the inner part of the mesopore channels. However, the hollow structures can reach a maximum storage capacity as long as the drug molecules can gain access to the cavities through any one of the accessible channels on the shell.

To date, researchers have extensively investigated HMS nanoparticles with improved drug loading and delivery properties. Shi and co-workers fabricated various spherical/ellipsoidal HMS nanostructures by a hard-templating route, micellar aggregate template route and co-templates route.<sup>74–78</sup> Fig. 3(A–C) gives the TEM images of typical HMS nanoparticles. Using IBU as a model drug,<sup>76</sup> they confirmed that the HMS nanostructures provide a significantly higher drug loading capacity, even reaching  $1133 \pm 52.4 \text{ mg g}^{-1}$ , which is three times higher than that of conventional mesoporous silica materials reported previously ( $337 \text{ mg g}^{-1}$ ). It is noteworthy that more than half of the drug is held in the hollow core and the storage capacity could also be adjusted in a wide range by the shell thickness.<sup>75</sup> The IBU loaded HMS SDDSs exhibit well sustained release properties, as the example shown in Fig. 3D. In addition, they developed a double shelled HMS spheres (HMSs@mSiO<sub>2</sub>) with different pore sizes, and the structure of the HMSs@mSiO<sub>2</sub> and HMS spheres (HMSs) is illustrated in Fig. 4B.<sup>40,79</sup> The surface area enlarges remarkably from 207 to  $1142 \text{ m}^2 \text{ g}^{-1}$  and the pore volume increases from  $0.37$  to  $0.93 \text{ cm}^3 \text{ g}^{-1}$  when the shell



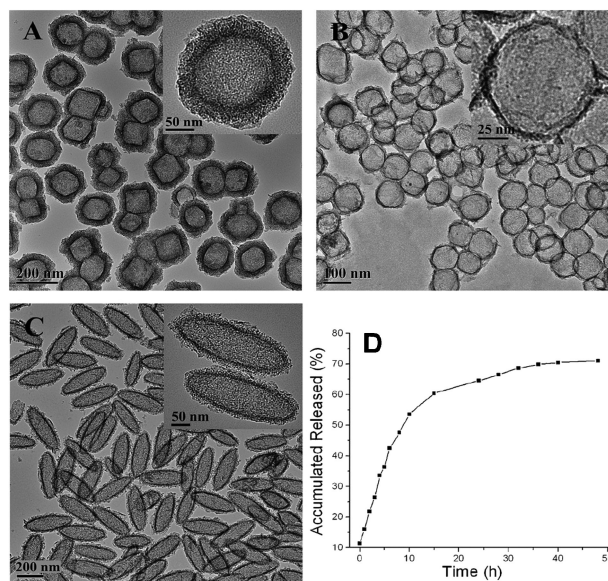


**Fig. 3** (A–C) TEM images at low and high (insets) magnifications of hollow mesoporous silica nanoparticles. (D) Ibuprofen release behavior in simulated body fluid over a 48 h period at 37 °C. (Adapted from ref. 74, Copyright 2009, Royal Society of Chemistry. Reproduced with permission.).

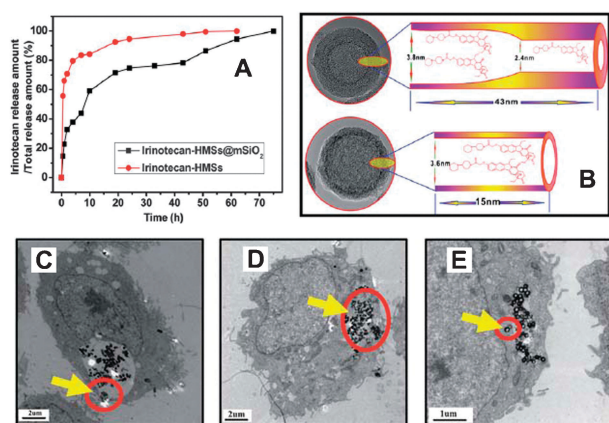


**Fig. 4** Irinotecan release profiles (A) from HMSs@mSiO<sub>2</sub> and HMSs; Schematic illustration (B) of the outward diffusion of irinotecan molecules inside the pore channels of HMSs@mSiO<sub>2</sub> and HMSs. Purposely selected bio-TEM images of HMSs@mSiO<sub>2</sub> uptake by MCF-7 cells (C–E) demonstrating that HMSs@mSiO<sub>2</sub> nanoparticles were firstly endocytosized to form a vesicle in the cell membrane (C), then in the endosomes (D) and later their endosomal escape into cytoplasm (E). (Adapted from ref. 40, Copyright 2011, Royal Society of Chemistry. Reproduced with permission.).

number increases from single to double. Compared to the conventional MCM-41 type mesoporous spherical silica nanoparticles with an uptake amount of 6.66% (surface area of 978 m<sup>2</sup> g<sup>-1</sup> and pore volume of 0.8 cm<sup>3</sup> g<sup>-1</sup>), the HMSs@mSiO<sub>2</sub> show a much higher anticancer drug loading capacity (15.24% anticancer drug docetaxel) due to the contribution of the hollow interior with enhanced drug loading capacity. The drug delivery results show that the deposition of a second mesoporous silica shell can lead to a more sustained release of anticancer drug (irinotecan) from the carriers (Fig. 4A), which can be explained

as the steric hindrance effect of the smaller pore size on the second shell and the longer releasing distance. In the bio-TEM images (Fig. 4C–E), drug loaded HMSs@mSiO<sub>2</sub> first enter cancer cells by the endocytosis effect to form a vesicle at the cell membrane, then the docetaxel loaded HMSs@mSiO<sub>2</sub> particles pass through endosomes and lysosomes, and are eventually released into the cytoplasm, revealing that the cell uptake mechanism for docetaxel-HMSs@mSiO<sub>2</sub> system is an endocytosis mechanism, which is more effective than the passive diffusion mechanism for free docetaxel. Therefore, the docetaxel molecules in the hollow cores diffuse through mesopore shells into the cytoplasm and cause cell death, which shows broad potential applications of the hollow structure in nanomedicine for cancer chemotherapy. Besides the above pure HMS materials, they also investigated the rattle-type HMS nanostructures with Au or Fe<sub>3</sub>O<sub>4</sub> as the core which possess both the properties of hollow structure and the functionalized core materials.<sup>41,73,80–82</sup> The rattle-type HMS nanostructures will be discussed in the next part of functional mesoporous silica material.

Zhu *et al.* reported another carbon-sphere template process to prepare HMS nanoparticles,<sup>83,84</sup> and then covalently grafting poly(oxyethylene) bis(amine) on the surfaces of HMS nanoparticles to form HMS-PEG nanoparticles. HMS-PEG nanoparticles have little *in vitro* cytotoxicity, and the uptake amount is approximately two times that of pure HMS nanoparticles in HeLa and NIH3T3 cells. Therefore, doxorubicin (DOX) loaded HMS-PEG nanoparticles have a slightly higher cytotoxicity than DOX loaded HMS nanoparticles against HeLa and NIH3T3 cells. The superior sustained release property is maintained, indicating that it is a promising strategy toward their potential application as drug delivery vehicles. Other HMS particles with interesting morphologies, such as rod-like HMS particles,<sup>85</sup> mesoporous silica nanotubes,<sup>86–89</sup> HMS nanocages with cubic shape,<sup>90</sup> and multi-shelled HMS nanoparticles<sup>91</sup> have also been reported. When used as drug carriers, all the HMS particles will be good candidates for absorption matrix and drug delivery carries due to their large pore volume (to store drug molecules) and nanometre (2–10 nm) pore size (to control the drug release rate).

### 3. Functional mesoporous silica SDDSs

With the rapid development of silica-based drug delivery systems over the past decades, the use of pure mesoporous silica suffers from limitations in many applications, such as (i) targeted drug delivery mechanisms study, (ii) drug kinetics marker in pharmacological research,<sup>92</sup> and (iii) track/evaluate the efficiency of the drug release in disease diagnosis and therapy. Therefore, functionalized mesoporous silica materials with luminescence and/or magnetism emerge as the times require. Different from the pure silica drug carriers, the smart combination of different functional materials can lead to the development of multifunctional medical platforms for simultaneous targeted delivery, fast diagnosis, and efficient therapy. In this part, we will review the luminescent, magnetic and bifunctional mesoporous silica SDDSs.

#### 3.1. Magnetism functionalized mesoporous silica SDDSs

Magnetic nanoparticles, an important class of inorganic materials, are especially attractive for targeted drug delivery application. Magnetic targeting provides the ability to guide

the drug delivery systems to the desired location, hold them until the therapy is complete, and then remove them by means of an external magnetic field.<sup>93</sup> This targeting ability is significant because many drugs, especially the cancer-therapy drugs, have toxic side effects. Targeted drug delivery systems can carry the drugs and be guided to the targeted organs or locations inside the body, which will facilitate the therapeutic efficiency and reduce the damage of normal organs or tissues due to the drug toxicity before targeting the desired positions.<sup>92,94</sup> Secondly, superparamagnetic nanoparticles can deliver certain amount of heat under alternating magnetic fields, as a result of Brownian rotation and Néel relaxation mechanisms, to reach hyperthermia temperatures for cancer treatment.<sup>95,96</sup> Among varieties of magnetic materials,  $\text{Fe}_2\text{O}_3$  and  $\text{Fe}_3\text{O}_4$  have been most intensively studied. However, pure iron oxide is prone to aggregation because of anisotropic dipolar attraction and rapid biodegradation when they are exposed to biological systems directly.<sup>97,98</sup> Thereby, iron oxide particles combined with mesoporous silica matrix is desirable in order to overcome the limitations and represent a significant advance in the field of drug delivery.<sup>35,37,99,100</sup> Recently, a significant breakthrough has been achieved on the synthesis of monodisperse iron oxide nanocrystals with superparamagnetism, high crystallinity, narrow size distributions, and dimensions on the order of 10 nm by high-temperature thermolysis of organometallic species.<sup>101–105</sup> These high-quality iron oxide nanocrystals are highly desirable for function-specific biological applications. Although the products obtained from the above approach are organic-soluble, treating with cationic surfactant CTAB has successfully transferred them to an aqueous for biological applications.<sup>99,106</sup>

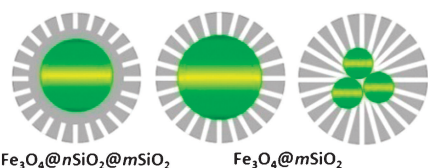
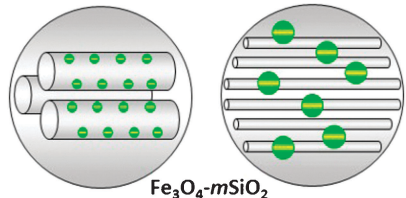
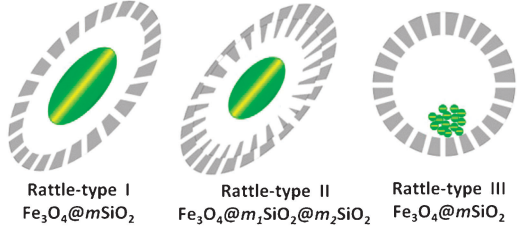
In recent years, fabrication of iron oxide-based magnetic mesoporous silica SDDSs has received much interest. According to the existing investigations, we group the iron oxide-based magnetic mesoporous silica materials into four basic structures.

The representative examples and structures are summarized in Table 2, including: (i) core-shell structure composites with mesoporous silica shell on the surface of iron oxide core; (ii) embedding iron oxide nanocrystals into mesoporous silica matrices; (iii) rattle-type hollow particles with iron oxide core and mesoporous silica shell; and (iv) capping the pores of mesoporous silica with iron oxide nanocrystals for stimuli-responsive CDDSs.

For the core-shell structure, the most straightforward synthetic strategy is the so-called bottom-up approach, where the core and shell are fabricated in an inside-to-outside order. Core-shell structure can provide the magnetic composites extremely high magnetization, even up to  $50 \text{ emu g}^{-1}$ .<sup>106,107</sup> As drug carriers, the outer mesoporous silica shell supplies enough surface area and pore volume for drug store and release. Shi *et al.* proved that the pore volume of the core-shell structured magnetic mesoporous silica SDDSs decrease 70% after IBU is stored, and the release can keep over 70 h,<sup>92</sup> showing potential application in targeted drug delivery and multiphase separation.

Very recently, we designed novel fibrous-structured mesoporous silica microspheres (denoted as  $\text{Fe}_3\text{O}_4/\text{FMSMs}$ , and insert Fig. 5A), which belong to the embedded structure. The  $\text{Fe}_3\text{O}_4/\text{FMSMs}$  exhibit a sustained drug release profile, sufficient magnetic responsivity and redispersibility to the external magnetic field (Fig. 5A and B). Seen from the intracellular

**Table 2** Structures of  $\text{Fe}_3\text{O}_4/\text{Fe}_2\text{O}_3$  functionalized mesoporous silica particles

Structures	Representative examples	Representative structures	Ref.
Core-shell structure	$\text{Fe}_3\text{O}_4@n\text{SiO}_2@m\text{SiO}_2$ sphere $\text{Fe}_3\text{O}_4@m\text{SiO}_2$ sphere (one core) $\text{Fe}_3\text{O}_4\text{-}x@m\text{SiO}_2$ sphere (several cores)		92, 107 106, 108–111 50, 112
Embedded structure	$\text{Fe}_x\text{O}_y$ -SBA-15 rice grain-like particle $\text{Fe}_x\text{O}_y$ -MCM-41 sphere $\text{Fe}_2\text{O}_3/\text{FeO}_x$ -SBA-16 $\text{Fe}_3\text{O}_4/\text{Fe}_2\text{O}_3$ - $m\text{SiO}_2$ sphere/nanorods $\text{Fe}_3\text{O}_4/\text{FMSMs}$ sphere		42, 113 114 115 116–118 27
Rattle-type hollow structure	$\text{Fe}_3\text{O}_4/\text{Fe}_2\text{O}_3@m\text{SiO}_2$ ellipsoids $\text{Fe}_3\text{O}_4/\text{Fe}_2\text{O}_3@m\text{SiO}_2$ ellipsoids (double mesoporous shells) $\text{Fe}_3\text{O}_4/\text{Fe}_2\text{O}_3@m\text{SiO}_2$ spheres (template method) $\text{Fe}_3\text{O}_4@m\text{SiO}_2$ spheres (hydrothermal etching)		80, 81 40 35, 44, 119 41, 73
$\text{Fe}_3\text{O}_4$ capped $m\text{SiO}_2$	$\text{Fe}_3\text{O}_4$ capped $m\text{SiO}_2$	(Shown in Table 3)	38, 45, 120

$n\text{SiO}_2$ : non-porous silica layer;  $m\text{SiO}_2$ : mesoporous silica layer; FMSMs fibrous-structured mesoporous silica microsphere.



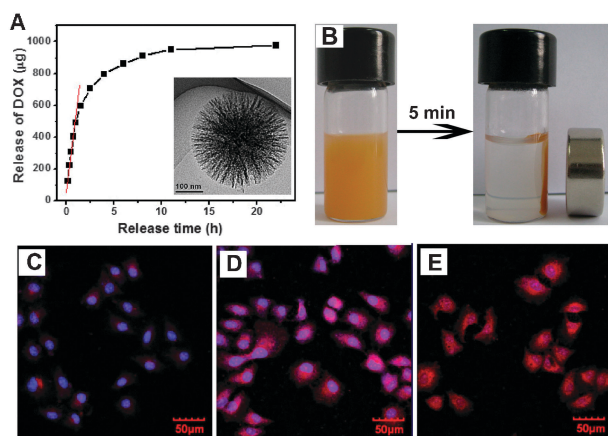


**Fig. 5** (A) Drug-release profile for DOX- $\text{Fe}_3\text{O}_4/\text{FMSMs}$  in PBS buffer. Inset is the TEM image of  $\text{Fe}_3\text{O}_4/\text{FMSMs}$ . (B) Photograph of the separation process of  $\text{Fe}_3\text{O}_4/\text{FMSMs}$  by a magnet. Confocal laser scanning microscopy (CLSM) images of HeLa cells incubated with DOX- $\text{Fe}_3\text{O}_4/\text{FMSMs}$  ([DOX] = 2 mM) for 10 min (C), 1 h (D), and 6 h (E) at 37 °C, the merged images of both the nuclei of cells (blue, being dyed by Hoechst 33324) and DOX fluorescence in cells (red). (Adapted from ref. 27, Copyright 2011, Royal Society of Chemistry. Reproduced with permission.).

drug delivery in Fig. 5C–E, DOX is observed both in the cell cytoplasm and cell nucleus, which indicates that DOX delivered by DOX- $\text{Fe}_3\text{O}_4/\text{FMSMs}$  can pass through the cytomembrane, assemble in cytoplasm, then pass through the nucleus membrane and eventually assemble in the nucleus to kill cells. Moreover, effective therapy of DOX may result from the enhanced intracellular delivery and the extracellular protection by DOX- $\text{Fe}_3\text{O}_4/\text{FMSMs}$ , showing that  $\text{Fe}_3\text{O}_4/\text{FMSMs}$  could be used as therapeutically effective drug delivery system for DOX delivery.

In the last five years, rattle-type particles with large hollow interior spaces, functional cores and mesoporous silica shells were designed and applied as controlled drug delivery carriers. Shi and co-workers prepared a series of rattle-type  $\text{Fe}_3\text{O}_4/\text{Fe}_2\text{O}_3@m\text{SiO}_2$  hollow ellipsoids/spheres with a single or double mesoporous silica shell (Rattle-type I and II in Table 2).<sup>40,41,73,80,81</sup> They proved that the saturation magnetization value of rattle-type hollow structure ( $35.7 \text{ emu g}^{-1}$ ) is evidently higher than that of the corresponding core-shell structure with an intact middle silica layer ( $28.8 \text{ emu g}^{-1}$ ) due to the removal of the in-between silica layer.<sup>41</sup> In addition, surface area and pore volume of the rattle-type structure are calculated to be  $435 \text{ m}^2 \text{ g}^{-1}$  and  $0.58 \text{ cm}^3 \text{ g}^{-1}$ , respectively, which are significantly higher than the sample with an intact middle silica layer ( $274 \text{ m}^2 \text{ g}^{-1}$  and  $0.38 \text{ cm}^3 \text{ g}^{-1}$ ). Therefore, compared with the core-shell structure and embedded structure which usually possesses low magnetism, the rattle-type structure is much suitable for targeting drug release. The typical structure of  $\text{Fe}_2\text{O}_3@m\text{SiO}_2@m\text{SiO}_2$  precursor and  $\text{Fe}_2\text{O}_3@m\text{SiO}_2$  hollow nanocapsule is given in Fig. 6A and B, respectively.<sup>80</sup> These nanocapsules possess sufficient magnetic responsivity (30 s complete magnetic field attraction) and high efficiency DOX loading ability (20%, attributed to the enhanced surface area and pore volume from the hollow interior). The excellent blood compatibility of  $\text{Fe}_3\text{O}_4@m\text{SiO}_2$  nanocapsules (Fig. 6C), and the greater cytotoxicity of DOX loaded

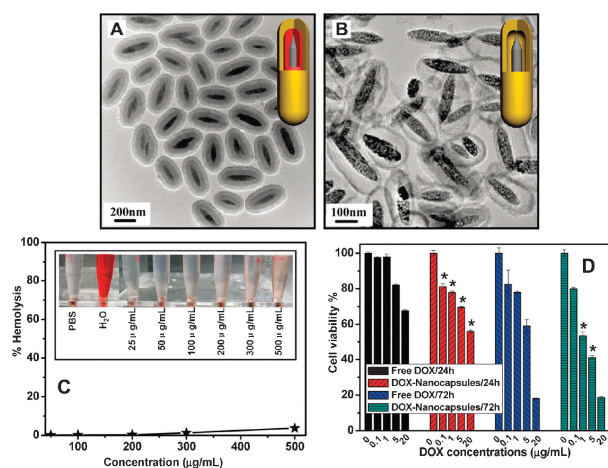


**Fig. 6** TEM images of ellipsoidal  $\text{Fe}_3\text{O}_3@m\text{SiO}_2@m\text{SiO}_2$  (A) and  $\text{Fe}_3\text{O}_4@m\text{SiO}_2$  (B); (C) Hemolysis assay for the magnetic nanocapsules (inset: photographic images for direct observation of hemolysis by the nanocapsules, using PBS as a negative control and water as positive control (the two tubes on the left), and the capsules suspended at different concentrations (the six tubes on the right)). The red blood cells are red due to the presence of hemoglobin in the RBCs. During the hemolysis assay experiment, hemoglobin will be released into the solution by hemolysis, resulting in visually red color in solution. (D) Cell viabilities of free DOX and DOX loaded  $\text{Fe}_3\text{O}_4@m\text{SiO}_2$  nanocapsules against MCF-7 cells at different concentrations for 24 and 72 h. (Adapted from ref. 80, Copyright 2010, American Chemical Society. Reproduced with permission.).

nanocapsules than free DOX to induce MCF-7 cell death (Fig. 6D), indicating that the  $\text{Fe}_3\text{O}_4@m\text{SiO}_2$  nanocapsules are excellent anticancer drug carriers for diagnosis and chemotherapy applications. Zhu and co-workers synthesized another rattle-type  $\text{Fe}_3\text{O}_4@m\text{SiO}_2$  hollow mesoporous silica sphere using carbon spheres as templates<sup>35,44,119</sup> (Rattle-type III in Table 2). The DOX loaded  $\text{Fe}_3\text{O}_4@m\text{SiO}_2$  hollow system have a sustained release property, and are useful for cases that require a high initial dose followed by a more stable release of smaller doses.  $\text{Fe}_3\text{O}_4$  capped mesoporous silica materials for stimuli-responsive CDDSs will be summarized in the Part 4.

### 3.2. Luminescence functionalized mesoporous silica SDDSs

It is well known that luminescent labelling is a real-time, simple, and effective way to monitor the route of drug-transport carriers in a living system. Therefore, luminescence functionalized mesoporous silica SDDSs which can be easily identified, tracked and monitored to evaluate the efficiency of the drug release and disease therapy have become a research hot spot.<sup>121,122</sup> Currently, the investigated or employed luminescent emitters have been focused on organic dyes, semiconductor nanocrystals, and rare-earth nanophosphors.

Traditionally, most of the biological luminescent labels are organic dyes, such as fluorescein isothiocyanates (FITC), rhodamine, and cyanine dyes (Cy3, Cy5, and Cy7). However, dye molecules usually suffer from photobleaching and quenching when exposed to harsh environments due to interactions with solvent molecules and reactive species such as oxygen or ions dissolved in solution.<sup>123</sup> Therefore, they are not very suitable for sensitive detection and real-time monitoring.<sup>7</sup> A promising strategy



to overcome the above drawbacks is to form dye-doped silica composites, which highly enhance the fluorescence intensity than the corresponding single dye molecule.<sup>11,124,125</sup> The most common method is the use of co-condensation approach with the help of the dehydration reaction between 3-aminopropyltriethoxysilane and dye molecules.<sup>11,25,126–132</sup> Shi *et al.* introduced the co-condensation method to covalently graft rhodamine B (RhB) groups within the mesoporous channels of SBA-15 (RhB-Cc-SBA-15) for red fluorescent emission.<sup>11,25</sup> Compared with other dye-doped silica materials, the co-condensed RhB-Cc-SBA-15 possesses high dye doping amounts (0.096–0.153 mmol g<sup>-1</sup>), high fluorescence quantum yields (up to 88.1%), excellent photostability and high fluorescence detectivity. They also proved that the salvianolic acid B (SAB) loaded samples possess a much more significant SAB sustained-release capability than pure mesoporous silica materials. Cell viability, hemolysis and coagulation behaviour assay suggest non-cytotoxicity and good blood compatibility of the material. These results are encouraging from the perspective of moving the material platform into clinical trials. In addition, there are several other reports on the synthesis of a core-shell structure that contains a nonporous dye-doped silica core and a mesoporous silica shell, which also possesses sustained drug release properties and good compatibility.<sup>125,133,134</sup>

Semiconductor nanocrystals, known as quantum dots (QDs), are composed of atoms from groups II–VI or III–V of the periodic table and generally defined as particles having physical dimensions smaller than the exciton Bohr radius. During the past decade, QDs have gained considerable attention as labels in biological imaging and detections due to the following outstanding optical properties: high quantum yield, excellent photostability, size-dependent tunable fluorescence properties, narrow emission bandwidths (span the visible spectrum), and broad excitation spectra (allow simultaneous efficient excitation of all colors).<sup>135–141</sup> High-quality QDs are typically prepared at elevated temperatures in high boiling-point organic solvents, such as long alkyl chain tri-*n*-octylphosphine oxide (TOPO) and hexadecylamine (HDA),<sup>142–148</sup> therefore hydrophobic ligand-capped are not suitable for biological applications. Lately, Hyeon *et al.* developed a simple approach, employing CTAB as a secondary surfactant, to transfer them into water-soluble QDs.<sup>149</sup> The CTAB-stabilized QDs can act as seeds for the formation of spherical mesoporous silica particles with excellent optical properties. Gao and co-workers have succeeded in exploiting this method to prepare mesoporous silica-coated QDs with multicolor luminescence.<sup>150</sup> Hyeon and several other groups also applied QD functionalized mesoporous silica on drug delivery systems,<sup>87,149,151,152</sup> in which the luminescence is detectable and the release profiles could be tuned by the mesoporous silica. Moreover, QDs possess super-small and well-defined diameters ranging between 1.5 and 8 nm. Therefore, Lin *et al.* and Zhu *et al.* used QDs to cap the openings of the mesoporous channels in the stimuli-responsive CDDSs (in next part).<sup>7</sup> Although some reports have confirmed that QD functionalized mesoporous silica drug delivery systems offer relatively low cytotoxicity and high biocompatibility.<sup>152,153</sup> Chen *et al.* coated QDs with silica which successfully prevented the interaction of Cd, Se, Zn, and sulfur with proteins and DNA in the nucleus.<sup>154</sup> However, we still worry about the toxic

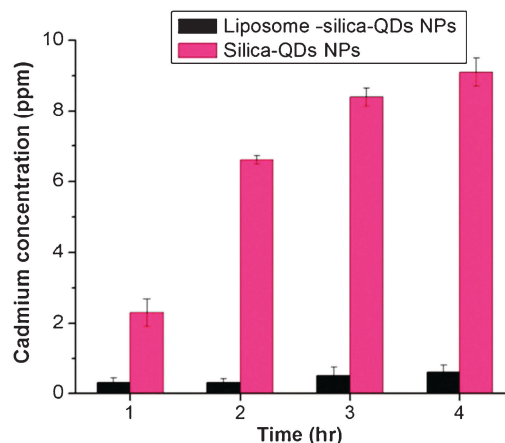


**Fig. 7** The *in vitro* release of cadmium ions from the QDs/mesoporous silica core-shell nanoparticles with or without PEGylated liposome coating. (Adapted from ref. 155, Copyright 2011, Royal Society of Chemistry. Reproduced with permission.)

heavy metals (such as Pb<sup>2+</sup> or Cd<sup>2+</sup>) released from the QDs as shown in Fig. 7.<sup>155</sup> In their elemental form, cadmium, selenium, zinc, and sulfur have all been known to cause nephro-toxicity or acute and chronic toxicities in living vertebrates.<sup>156</sup> Initial studies have even shown that QDs are not excreted and remain intact *in vivo*.<sup>157,158</sup> The natural and fatal shortcoming limits the applications of QDs, especially use in the human body.

Another excellent luminescent material is rare-earth (RE) based phosphors, which exhibit intense narrow-band intra-4f luminescence in a wide range of host materials. The shielding provided by the 5s<sup>2</sup> and 5p<sup>6</sup> electrons causes rare-earth radiative transition in solid hosts to resemble those of the free ions. Therefore, RE-doped nanophosphors holding the advantages of large Stokes shift, sharp emission spectra, long lifetime, high chemical/photochemical stability, low toxicity and reduced photobleaching over semiconductor nanocrystals and organic dye molecules,<sup>159–161</sup> seem to be a promising luminescent material for biological applications. Additionally, it is easy to realize multicolor luminescence using RE-doped nanophosphors by only changing the doped RE ions.<sup>162,163</sup>

Our group pioneeringly exploited RE-doped nanophosphors for sustained drug delivery, including hollow RE materials and RE functionalized mesoporous silica composites. The study on hollow RE particles (such as Yb(OH)CO<sub>3</sub>@YbPO<sub>4</sub> core-shell structure, CaF<sub>2</sub>:Ce<sup>3+</sup>/Tb<sup>3+</sup>, GdPO<sub>4</sub> and GdPO<sub>4</sub>:Eu<sup>3+</sup>),<sup>164–167</sup> especially the cell viability and inverted microscopy images of the cells grown in the study, proves the good biocompatibility of the hollow RE materials. The dissolving behavior of rare earth ions is another important factor for the actual application as a potential drug carrier. In the present study, the drug storage-release experiment reveals that the phase structure and photoluminescence of the hollow RE materials vary little before and after the drug storage-release measurement, indicating the good stability of the RE materials in phosphate buffer solution or acetate buffer solution. The above results indicate that the RE materials have low or non-toxicity and are promising for biomedical application.

The structures classified in Table 2 for magnetic mesoporous silica materials can also be employed to assort

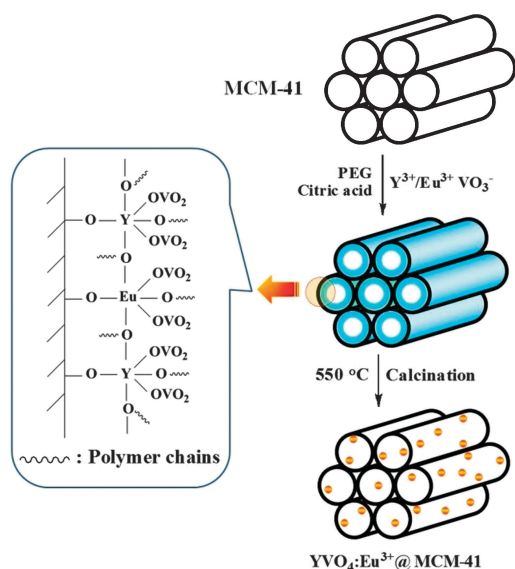


**Fig. 8** Scheme illustrating the luminescence functionalization of MCM-41 by  $\text{YVO}_4:\text{Eu}^{3+}$  through sol-gel process.

the RE functionalized mesoporous silica composites, for example, embedded structure and core-shell structure. The embedded structure is to deposit phosphor nanocrystals into the channels of the well known mesoporous silica particles including MCM-41, MCM-48 and SBA-15.<sup>59,163,168–170</sup> The typical synthesis process of  $\text{YVO}_4:\text{Eu}^{3+}$  functionalized MCM-41 (denoted as  $\text{YVO}_4:\text{Eu}^{3+}@\text{MCM-41}$ ) composites through sol-gel process is presented in Fig. 8. Although the method will block the pores to some extent, the special high surface area and pore volume of the chosen mesoporous materials still offer the luminescent materials a high surface area ( $750\text{--}1300\text{ m}^2\text{ g}^{-1}$ ) and pore volume (around  $0.8\text{ m}^3\text{ g}^{-1}$ ) for drug loading and sustained release (Fig. 9A).<sup>168</sup> Moreover, the emission of  $\text{RE}^{3+}$  ions will be quenched in the environments which contain a high phonon frequency.<sup>171</sup> Therefore, on the one hand, in drug molecule IBU loaded systems ( $\text{IBU-YVO}_4:\text{Eu}^{3+}@\text{MCM-41}$ ), the organic groups in IBU with vibration frequencies from  $1000$  to  $3250\text{ cm}^{-1}$  will greatly quench the emission of  $\text{Eu}^{3+}$  in all the drug loaded systems. On the other hand, the quenching effect on the emission of  $\text{Eu}^{3+}$  will be weakened with the release of IBU, which results in the increase of emission intensity (Fig. 9B). This relationship between the emission intensity and drug release extent allows the drug release process to be monitored and tracked by the change of photoluminescence intensity. Another example is to deposit  $\text{CaWO}_4:\text{Ln}$  ( $\text{Ln} = \text{Eu}^{3+}, \text{Dy}^{3+}, \text{Sm}^{3+}, \text{Er}^{3+}$ ) phosphor nanocrystals into MCM-41.<sup>163</sup> As mentioned before, multicolour (red, yellow, blue and orange) luminescence comes from the characteristic emission spectra of different doped ions,  $\text{Eu}^{3+}, \text{Dy}^{3+}, \text{Sm}^{3+}$  and  $\text{Er}^{3+}$ . Also, this system exhibits sustained drug release profiles. These results are encouraging from the perspective of moving the RE functionalized mesoporous silica systems into luminescent labelling to evaluate the efficiency of the drug release and disease therapy. Another way to form a core-shell structure by coating phosphor core with ordered mesoporous silica shell was explored to reduce the interference of the environment on the luminescent property of the phosphor core and completely

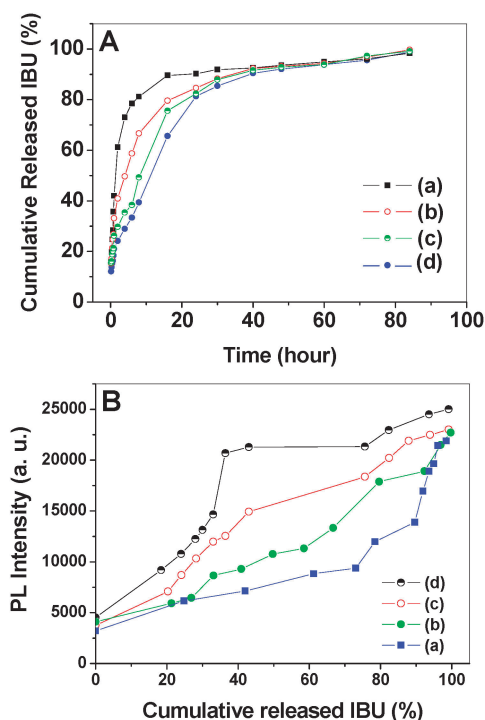


**Fig. 9** (A) Cumulative IBU release profiles from  $\text{IBU-YVO}_4:\text{Eu}^{3+}@\text{MCM-41-A}$  (a),  $\text{IBU-YVO}_4:\text{Eu}^{3+}@\text{MCM-41-B}$  (b),  $\text{IBU-YVO}_4:\text{Eu}^{3+}@\text{MCM-41-C}$  (c), and  $\text{IBU-YVO}_4:\text{Eu}^{3+}@\text{MCM-41-D}$  (d) systems in the release media of SBF. (B) The PL emission intensity of  $\text{Eu}^{3+}$  in  $\text{IBU-YVO}_4:\text{Eu}^{3+}@\text{MCM-41-A}$  (a),  $\text{IBU-YVO}_4:\text{Eu}^{3+}@\text{MCM-41-B}$  (b),  $\text{IBU-YVO}_4:\text{Eu}^{3+}@\text{MCM-41-C}$  (c), and  $\text{IBU-YVO}_4:\text{Eu}^{3+}@\text{MCM-41-D}$  (d) as functions of cumulative release amount of IBU. (Adapted from ref. 168, Copyright 2007, Elsevier Ltd. Reproduced with permission.)

utilize the excellent advantages of the silica matrix. We have coated  $\text{Y}_2\text{O}_3:\text{Eu}$ ,  $\text{CeF}_3:\text{Tb}$ , and  $\text{Gd}_2\text{O}_3:\text{Eu}$  core with mesoporous silica shell.<sup>26,162,172,173</sup> All the systems exhibit sustained drug release profiles and excellent luminescent properties. For core-shell structured  $\text{Gd}_2\text{O}_3:\text{Eu}^{3+}@\text{nSiO}_2@\text{mSiO}_2$  nanocomposite,<sup>26</sup> research on biocompatibility shows that it is non-toxic, while the DOX-loaded system exhibits an even greater cytotoxicity than free DOX (Fig. 10A and B). The fragmented HeLa cell nuclei treated with  $\text{DOX-Gd}_2\text{O}_3:\text{Eu}^{3+}@\text{nSiO}_2@\text{mSiO}_2$  (Fig. 10C and D) clearly reveal the activity of the loaded DOX with the mechanisms of killing tumor cells by DNA damage and topoisomerase II inhibition. These preliminary results favor the potential applications of the core-shell structure in the fields of drug delivery and disease therapy. It should be pointed out that infrared-to-visible up-conversion phosphors with high photo-stability, high detection sensitivity, and reduced instrument cost have been a research hot spot.<sup>174–177</sup> Different from the down-conversion phosphors which emit low energy fluorescence when excited by high energy light, up-conversion phosphors can emit a higher energy photon after absorbing two or more lower energy excitation photons on the basis of sequential adsorption and energy transfer steps.<sup>178</sup> The use of lower energy light is associated with several significant advantages such as negligible photodamage to living organisms, good biocompatibility, and high light excitation-penetration depths of near-infrared (NIR) irradiation in tissues.<sup>179–181</sup>

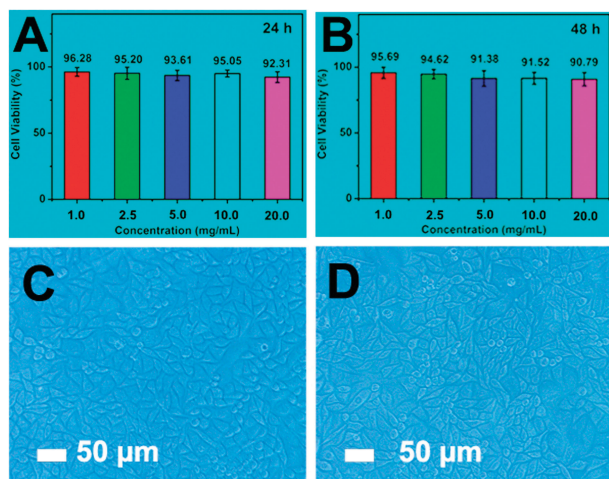


**Fig. 10** (A) Cytotoxicity of DOX, DOX-Gd<sub>2</sub>O<sub>3</sub>:Eu<sup>3+</sup>@nSiO<sub>2</sub>@mSiO<sub>2</sub>, and Gd<sub>2</sub>O<sub>3</sub>:Eu<sup>3+</sup>@nSiO<sub>2</sub>@mSiO<sub>2</sub> on HeLa cells after 24 h and (B) 48 h. (C) The nucleus of blank HeLa cells. (D) The nucleus of HeLa cells incubated with DOX-Gd<sub>2</sub>O<sub>3</sub>:Eu<sup>3+</sup>@nSiO<sub>2</sub>@mSiO<sub>2</sub> for 12 h. (Adapted from ref. 26, Copyright 2011, Royal Society of Chemistry. Reproduced with permission.)

Furthermore, excitation with the NIR only results in a very weak autofluorescence background because the UV-excitable biomolecules (biological tissues and fluorescent drug molecules) which interfere with normal phosphor luminescence can no longer be excited by NIR radiation.<sup>182–184</sup> To increase the NIR absorption strength of upconversion lanthanide ions in host lattice, Yb<sup>3+</sup> is often co-doped with the other ions (Er<sup>3+</sup>, Tm<sup>3+</sup>, and Ho<sup>3+</sup>), as a sensitizer for the upconversion process. It is also noted that the rare earth elements used in the synthesis have a lower toxicity than the semiconductor elements of QDs (the 50% lethal dosage is approximately a thousand times higher than that of QDs), while the up-conversion fluorescence is much stronger than that of QDs.<sup>185,186</sup> These merits endow this kind of phosphor with potential as alternatives for dyes and QDs. Thus, we designed core-shell structured NaYF<sub>4</sub>:Yb<sup>3+</sup>/Er<sup>3+</sup>@nSiO<sub>2</sub>@mSiO<sub>2</sub> and Gd<sub>2</sub>O<sub>3</sub>:Er<sup>3+</sup>@nSiO<sub>2</sub>@mSiO<sub>2</sub> drug carriers by coating non-porous and further mesoporous SiO<sub>2</sub> layers with different thicknesses on upconversion NaYF<sub>4</sub>:Yb<sup>3+</sup>/Er<sup>3+</sup> and Gd<sub>2</sub>O<sub>3</sub>:Er<sup>3+</sup> nanophosphors.<sup>187,188</sup> Taking NaYF<sub>4</sub>:Yb<sup>3+</sup>/Er<sup>3+</sup>@nSiO<sub>2</sub>@mSiO<sub>2</sub> (denoted as NaSiSi) nanosphere as an example, different thicknesses of the mesoporous SiO<sub>2</sub> layers on the NaYF<sub>4</sub>:Yb<sup>3+</sup>/Er<sup>3+</sup> nanoparticles result from the different volume of TEOS (0.10, 0.15, and 0.30 mL) added during the experimental process (Fig. 11A). Upon excitation by a 980 nm near-infrared laser, the systems emit green (<sup>2</sup>H<sub>11/2</sub>, <sup>4</sup>S<sub>3/2</sub> → <sup>4</sup>I<sub>15/2</sub>) and red (<sup>4</sup>F<sub>9/2</sub> → <sup>4</sup>I<sub>15/2</sub>) fluorescence of Er<sup>3+</sup> even after the loading of IBU (Fig. 11B). Notably, the drug release amount and process can be monitored by the change of the up-conversion emission intensity. It is reasonable that the sample with the thickest mesoporous silica shell, providing the longest diffusion path and highest diffusion resistance, exhibits the slowest drug release rate (Fig. 11C). Recently, monodisperse and well-defined up-conversion phosphors have been successfully prepared *via* decomposition route in high boiling solvent.<sup>189–195</sup> We synthesized oleic acid capped NaYF<sub>4</sub>:Yb<sup>3+</sup>/Er<sup>3+</sup> nanocrystals and

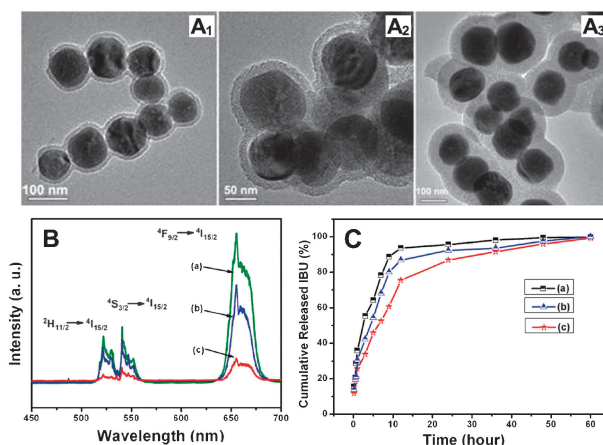


**Fig. 11** TEM images of NaSiSi-0.10 (A<sub>1</sub>), NaSiSi-0.15 (A<sub>2</sub>), and NaSiSi-0.30 (A<sub>3</sub>); (B) Visible up-conversion spectra of NaYF<sub>4</sub>:Yb<sup>3+</sup>/Er<sup>3+</sup> (a), NaSiSi-0.15 (b), and IBU-NaSiSi-0.15 (c). (C) Cumulative IBU release from IBU-NaSiSi-0.10 (a), IBUNaSiSi-0.15 (b), and IBU-NaSiSi-0.30 (c) systems in the release media of SBF. (Adapted from ref. 187, Copyright 2011, American Chemical Society. Reproduced with permission.)

transferred them into water according to literature.<sup>149</sup> Then NaYF<sub>4</sub>:Yb<sup>3+</sup>/Er<sup>3+</sup>@mSiO<sub>2</sub> fibers were obtained by electrospinning using water-soluble NaYF<sub>4</sub>:Yb<sup>3+</sup>/Er<sup>3+</sup> nanocrystals as fluorescent component. This new type of drug delivery carrier shows good biocompatibility and sustained release properties.<sup>196</sup>

### 3.3. Multifunctional mesoporous silica SDDSs

New strategy for the development of next generation silica carrier is to fuse luminescence and magnetism into one mesoporous silica matrix. The multifunctional material can favorably seek the diseased tissues and visualize the drug delivery system in real time when controllably releasing the drugs. The process can be abbreviated as “find-detect-treat” in one body. Furthermore, high performance in specific biological applications require that the multifunctional composites possess some unique features, such as suitable particle size, spherical morphology, narrow size distribution, large surface area (for drug, maximal protein, or enzyme binding), and high saturation magnetization to provide maximum signal.<sup>197–199</sup>

We designed the core-shell structured multifunctional nanocomposites using silica-coated Fe<sub>3</sub>O<sub>4</sub> nanospheres as core, ordered mesoporous silica as shell, and further deposition of phosphors (down-conversion YVO<sub>4</sub>:Eu<sup>3+</sup> or up-conversion NaYF<sub>4</sub>:Yb,Er/Tm phosphor nanocrystals).<sup>100,200</sup> The synthesis process of Fe<sub>3</sub>O<sub>4</sub>@nSiO<sub>2</sub>@mSiO<sub>2</sub>@NaYF<sub>4</sub>:Yb,Er is presented in Fig. 12(A). The obtained core-shell structured system exhibits unique green up-conversion emission under 980 nm laser excitation even after loading with drug molecules, high magnetization (38.0 emu g<sup>-1</sup>, 30 s response to foreign magnetic field) and a sustained drug release property (Fig. 12B–E). The up-conversion emission intensity of the multifunctional carrier also increases with the released amount of model drug, thus allowing the release process to be monitored and tracked by the change of photoluminescence intensity (Fig. 12F). This composite can act as a multifunctional drug carrier system, which can target and monitor drugs simultaneously and could



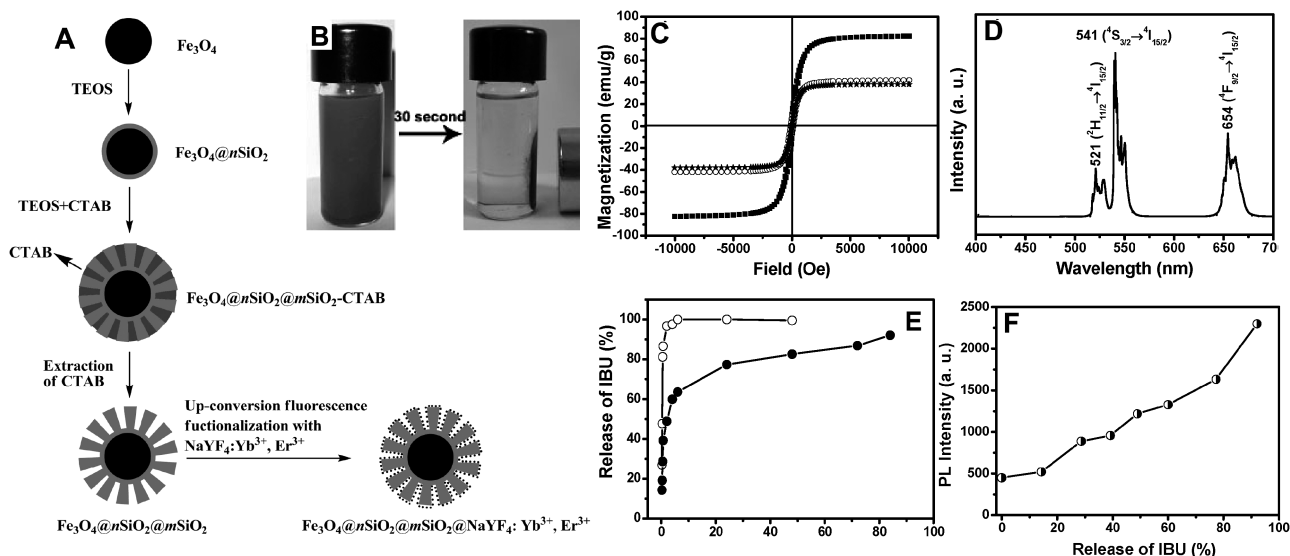


**Fig. 12** (A) The formation process of multifunctional  $\text{Fe}_3\text{O}_4@n\text{SiO}_2@m\text{SiO}_2@n\text{NaYF}_4:\text{Yb}^{3+}, \text{Er}^{3+}$  nanocomposites. (B) The separation process of the  $\text{Fe}_3\text{O}_4@n\text{SiO}_2@m\text{SiO}_2@n\text{NaYF}_4:\text{Yb}^{3+}, \text{Er}^{3+}$  by a magnet. (C) The magnetic hysteresis loops of pure  $\text{Fe}_3\text{O}_4$  (■),  $\text{Fe}_3\text{O}_4@n\text{SiO}_2@m\text{SiO}_2$  (○), and  $\text{Fe}_3\text{O}_4@n\text{SiO}_2@m\text{SiO}_2@n\text{NaYF}_4:\text{Yb}^{3+}, \text{Er}^{3+}$  (★). (D) Up-conversion emission spectra of  $\text{Fe}_3\text{O}_4@n\text{SiO}_2@m\text{SiO}_2@n\text{NaYF}_4:\text{Yb}^{3+}, \text{Er}^{3+}$  nanocomposites excited by 980 nm IR light. (E) Cumulative IBU releases from the IBU- $\text{Fe}_3\text{O}_4@n\text{SiO}_2@m\text{SiO}_2@n\text{NaYF}_4:\text{Yb}^{3+}, \text{Er}^{3+}$  (○) and IBU- $\text{Fe}_3\text{O}_4@n\text{SiO}_2@m\text{SiO}_2@n\text{NaYF}_4:\text{Yb}^{3+}, \text{Er}^{3+}-\text{NH}_2$  (●) systems versus release time. (F) Up-conversion emission intensity of  $\text{Er}^{3+}$  in IBU- $\text{Fe}_3\text{O}_4@n\text{SiO}_2@m\text{SiO}_2@n\text{NaYF}_4:\text{Yb}^{3+}, \text{Er}^{3+}$  as a function of the cumulative released IBU. (Adapted from ref. 100, Copyright 2010, WILEY-VCH Verlag GmbH & Co. KGaA, Weinheim. Reproduced with permission.)

be a new candidate of the “find-detect-treat” carrier. In addition, by coating  $\text{Fe}_3\text{O}_4@n\text{SiO}_2@m\text{SiO}_2$  with Au particles, another multifunctional mesoporous silica material exhibiting near-infrared absorption has been achieved,<sup>201</sup> and is suitable for targeting drug delivery and photothermal therapy.

In addition, other multifunctional mesoporous silica SDDSs have also been developed. For example, Zink *et al.* and Hyeon *et al.* successfully prepared  $\text{Fe}_3\text{O}_4/\text{Dye}/m\text{SiO}_2$  SDDSs.<sup>37,129</sup> In these systems, dye is doped in a mesoporous silica matrix, and  $\text{Fe}_3\text{O}_4$  nanoparticles are designed as the core in the center or satellites on the surface. Shi *et al.* and Hyeon *et al.* synthesized other types of  $\text{Fe}_3\text{O}_4/\text{QDs}/m\text{SiO}_2$  SDDSs: (i)  $\text{Fe}_3\text{O}_4$  and CdSe/ZnS QDs simultaneously embedded in mesoporous silica matrix,<sup>149</sup> and (ii) CdTe QDs self-assembled onto the surface of  $\text{Fe}_3\text{O}_4@m\text{SiO}_2@m\text{SiO}_2$  nanoparticles.<sup>152</sup>

#### 4. Stimuli-responsive CDDSs

As mentioned before, SDDSs with simple physical adsorption of drug molecules into the channels of mesoporous silica materials will cause immediate drug release after administration.<sup>202–204</sup> In cancer therapy, to achieve complete eradication of tumors, anticancer drugs must be administrated systematically in high dose to ensure the sufficient and sustained therapy efficiency. While, SDDSs will cause severe side-effect due to the non-specific uptake of anticancer drugs by healthy tissues/organs such as liver, kidney, bone marrow and heart before reaching the targeted organs or tissues.<sup>80</sup> It means that an ideal drug carrier should encapsulate the anticancer drugs with high loading amount and efficiency, and possess “zero release” effect prior to reaching the targeted cells to protect the healthy organs from the toxic drugs and prevent the decomposition/denaturing of the drugs. Therefore, it is highly desirable to

design CDDSs in which the drug-loading mesopores of these materials can be closed and opened at will. This breakthrough has been realized by stimuli-responsive CDDSs. In this system, the mesopores loaded with drug molecules can be capped by various “gatekeepers”. Being blocked, drug molecules are unable to be leach out from the mesoporous silica host, thus preventing any premature release. The release is triggered only upon exposure to stimuli, which induce the removal of gatekeepers and then release of the pore-entrapped drug molecules.

To date, diverse types of gatekeepers, such as nanoparticles (NPs), macrocyclic molecules, liner molecules and polymer multilayers, have been investigated. Table 3 summarizes the major types and structures of the used gatekeepers. In the NPs-gatekeeping systems (Structure I), solid NPs were chemically attached on the pore outlets of modified mesoporous silica, and could be removable with various external stimuli to destroy the chemical bonds, such as pH, redox potential and temperature. Macrocyclic organic molecules (Structure II) and liner molecules (Structure III) systems rely on supramolecular chemistry, which is a powerful methodology for the construction of various molecular devices, here, supramolecular gatekeepers. Macrocyclic organic molecule gatekeepers were realized by assembling movable macrocyclic molecules ( $\alpha$ - or  $\beta$ -cyclodextrin, cucurbit[6]uril, and dibenzo-24-crown-8) on immobilized stalks to form supramolecular caps on the pore outlets. The supramolecular caps can be disassembled by external stimuli to release the trapped drug molecules. For liner molecular gatekeepers, stimuli-responsive linear supermolecules are anchored to the external surface of mesoporous materials, and the “close/open” mechanism arises from “across/parallel or shorten” of the liner molecules. Structure IV coats the mesoporous silica with stimuli-responsive polymer layers, biomolecules or polyelectrolyte multilayers to cap the mesopore channels. When the system is stimulated, the multilayers will open

**Table 3** Different gatekeepers on the pores of mesoporous silica composites in stimuli-responsive CDDSs

Classes	Examples	Schematic structures	Ref.
<b>Structure I</b> nanoparticles (NPs)	Au NPs CdS NPs Fe <sub>3</sub> O <sub>4</sub> NPs ZnO NPs	<p>Functionalized NPs Drug molecule Modification group Mesoporous silica</p>	39, 58 7 38, 45, 120 205
<b>Structure II</b> macrocylic organic molecules	Cyclodextrin (CD) Cucurbit[6]uril (CB[6]) Dibenzo-24-crown-8 (DB24C8)	<p>α-CD CB[6] Stalk CD BD24C8</p>	36, 52, 55, 206–210 54, 208, 211, 212 208, 213
<b>Structure III</b> liner molecules	Liner polyamine Saccharide derivative Liner polymer Peptide sequence	<p>Liner molecules</p>	53, 62 214–216 217 218
<b>Structure IV</b> multilayers shell coating	Polymer layers Biomolecules Polyelectrolyte multilayers	<p>Mesoporous silica</p>	83, 219–221 63, 222 43, 47
<b>Structure V</b> pores modification	Functional molecule Polymer Azobenzene derivatives impeller	<p>(a) Functional molecule or polymer (b) Nanoimpeller</p>	61, 223, 224 225–227 211, 228

the pathways for drug molecule diffusion out. In addition, there are also few reports on functionalization of the pore interiors with stimuli-responsive polymers or nanoimpellers (Structure V).

#### 4.1. pH-responsive CDDSs

Among vigorous stimuli-responsive CDDSs, biological pH-responsive drug delivery systems received the most investigation since the human body exhibits variations in pH along the gastrointestinal tract from the stomach (pH = 1.0–3.0), to the small intestine (pH = 6.5–7.0), then to the colon (pH = 7.0–8.0).<sup>229</sup> In addition, cancer cells have a more acidic environment compared with normal cells.<sup>230,231</sup> These pH sensitive human systems and tissues provide an efficient way to control the drug release behavior by pH stimuli.

Zink and co-workers developed several pH-responsive mesoporous silica CDDSs utilizing the pH-dependent pseudorotaxanes, rotaxanes or other analogues. In these systems, the aromatic amines/ammonium stalks were immobilized on the surface of mesoporous silica nanoparticles (MSNP), and macrocyclic movable gates were introduced to encircle the stalks for controlling the flow of the drug models loaded in the pore channels (Structure II). For instance, the efficient macrocyclic

movable gate  $\beta$ -cyclodextrin ( $\beta$ -CD) was developed by Zink and co-workers.<sup>36</sup> The nanovalve formation and cap release mechanism is given in Fig. 13. The  $\beta$ -CD rings encircle aromatic amine stalks as a result of non-covalent bonding interactions under neutral pH conditions, and effectively block the nanopore openings and trap the included drug molecules. Decreasing the pH under mildly acidic conditions leads to protonation of the aromatic amines and dissociation of  $\beta$ -CD caps, following drug models diffusion from the nanopores. The drug release profiles before and after acid stimuli is shown in Fig. 14a, which present typical stimuli-responsive release properties: ability to contain drug molecules before stimuli but release them with response to the stimuli. The slow and incomplete release of DOX has been improved greatly by modifying MSNP with 7.5% ammonium (Fig. 14b). In KB-31 cells, DOX loaded nanoparticles are efficiently taken up into acidifying endosomal compartments (Fig. 14c), resulting in the cells going through endocytosis at 3 h, apoptosis by 60 h, nuclear fragmentation after 80 h, and finally cell death. The fact supports that the cargo release is caused by lysosomal acidification, which demonstrates the feasibility of the *in vitro* operation of the pH-sensitive nanovalves.

Martínez-Máñez *et al.* tethered the well-known pH-responsive linear polyamine molecules on the pore outlets of MCM-41

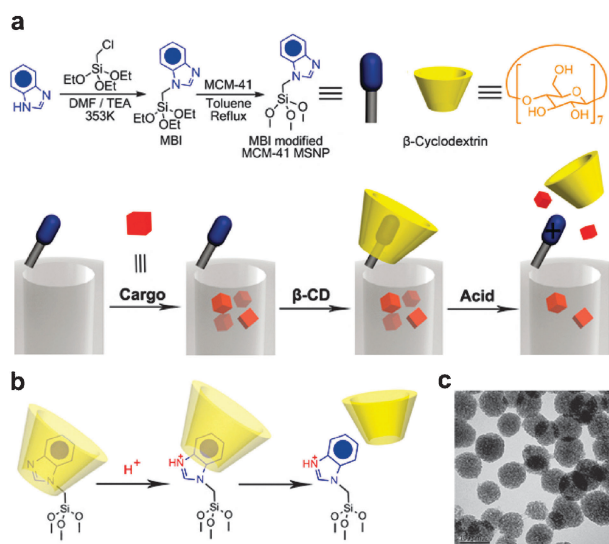


**Fig. 13** A graphical representation of the pH responsive MSNP nanovalve. (a) Synthesis of the stalk, loading of the cargo, capping of the pore, and release of the cap under acidic conditions. Based on previous calculations, the maximum number of stalks per nanopore is 6, and the maximum number of fully assembled nanovalves per nanopore is 4. The average nanopore diameter of the MSNP is around 2.2 nm, and the periphery diameter of the secondary side of  $\beta$ -cyclodextrin is about 1.5 nm. Thus, for a cargo with a diameter  $>0.7$  nm, a single nanovalve should be adequate to achieve effective pH-modulated release. (b) Details of the protonation of the stalk and release of the  $\beta$ -cyclodextrin. (c) TEM image of capped MSNP. The scale bar is 100 nm. (Adapted from ref. 36, Copyright 2010, American Chemical Society. Reproduced with permission.)

material through covalent bonds (Structure III),<sup>53,62</sup> resulting in both pH-controlled and anion-controlled gate-like effects. The pH-controlled “open/close” mechanism arises from hydrogen-bonding interactions between amines at neutral pH and Coulombic repulsions in closely located polyammoniums at acidic pH. The anion-controllable response can be explained in terms of anion complex formation with the tethered polyamines. They also concluded that the introduction of the larger anions (such as fluoride anion) results in a more compact arrangement of the polyamines, resulting from the interaction (formation of complexes) between the protonated amines and anion. MCM-41 functionalized with Saccharides at the pore outlets, then capped with anion borate and boronic acid functionalized gold nanoparticle for pH-responsive CDDSs have also been reported by Martínez-Mañez *et al.*<sup>58,214</sup>

Besides, employing hollow mesoporous silica spheres as container, Shi *et al.* designed a novel pH-responsive CDDSs by using polycation poly (allylamine hydrochloride)/sodium polystyrene sulfonate (PAH/PSS) polyelectrolyte multilayers as a coating shell to cap the mesopore openings of drug-loaded hollow spheres (Structure IV).<sup>43,47</sup> The negatively charged mesoporous silica surface favors a first-layer coating of the positively charged polycation PAH, and then the negatively charged PSS. Because of the pH sensitivity and salt-induced responsive property of the PAH/PSS multilayers, they can be used in stimuli-responsive CDDSs. It is encouraging that the system has both the advantages of high storage capacity of drug molecules (three times higher than that of the widely used MCM-41) and pH-responsive storage/release property.

## 4.2. Redox-responsive CDDSs

Redox reactions have been another popular stimulus to control mass transport in mesoporous materials. Lin and co-workers have creatively developed a series of redox-responsive mesoporous silica CDDSs, in which CdS nanoparticles,<sup>7</sup>  $\text{Fe}_3\text{O}_4$  nanoparticles,<sup>120</sup> and poly(amido amine) dendrimers<sup>232</sup> were used as the gatekeepers to cap the pores, and various disulfide-reducing agents as release triggers (Structure I). As an example of CdS nanoparticles capped mesoporous silica nanosphere (MNS) redox-responsive CDDS (Fig. 15), 2-(propyldisulfanyl) ethylamine groups on the surface of the open mesopores covalently capture the water-soluble mercaptoacetic acid-derivatized CdS nanocrystals, resulting in disulfide linkages. The linkages are chemically labile in nature and can be cleaved with various disulfide-reducing agents, such as dithiothreitol (DTT) and mercaptoethanol (ME). Hence, the release of the CdS nanoparticle caps from the drug-loaded MSNs can be regulated by introducing various amounts of release triggers. CdS-capped MCM-41 CDDS exhibits less than 1.0% of drug release over a period of 12 h in Fig. 16a, demonstrating a good capping efficiency of the CdS nanoparticles. Addition of DTT disulfide-reducing molecules to the aqueous suspension of CdS-capped mesoporous silica nanospheres triggered a rapid release of the mesopore-entrapped drug, reaching 85% within 24 h. Moreover, the release rate can be dictated by the removal rate of CdS caps due to the similar DTT concentration dependencies (Fig. 16b), and the removal rate of CdS caps can be detected easily by the luminescence. Seen from the effect of adenosine triphosphate (ATP) release from CdS-capped MSNs in astrocytes (Fig. 16c), perfusion application of ME results in a drastic decrease in the fluorescence intensity of CdS at the areas of the ATP-loaded MSN piles (MSN-1 and MSN-2), indicating (i) the CdS caps have been released and diffused away from the surface-bound MSNs and (ii) the released ATP molecules (from MSN-1 pile) have reached their receptors on the cell surface of those astrocytes (Cell-1 and -2) located at the downstream areas of the flow. So, the system could play a significant role in developing new generations of site-selective, controlled-release delivery, and interactive sensory nanodevices.

For the  $\text{Fe}_3\text{O}_4$  nanoparticle capped stimuli-responsive CDDS,<sup>120</sup> the disulfide linkages between the MSNs and the  $\text{Fe}_3\text{O}_4$  nanoparticles can be cleaved with various cell-produced antioxidants and disulfide reducing agents, presenting the similar capping efficiency and release properties to CdS-capped MSNs. It is noted that the entire  $\text{Fe}_3\text{O}_4$ -capped MSN carrier system can be magnetically directed to the site where the release should take place by applying an external magnetic field to realize targeting. Further studies of the redox-responsive CDDSs capped with generation 2.5 poly (amido amine) dendrimers (G2.5 PAMAM), which is smaller than the pore diameter, show a more gradual and plateau-like release profile to CdS-capped CDDSs.<sup>232</sup> The advantages of G2.5 PAMAM caps can be explained as following: (i) the flexible G2.5 PAMAM caps can flex slightly and form more bonds to the pore, (ii) bind more than one G2.5 PAMAM cap inside the pores, both resulting in more and tighter disulfide bonds to be broken. Consequently, decreasing the drug release rate significantly. More importantly, the commercially available PAMAM dendrimers are



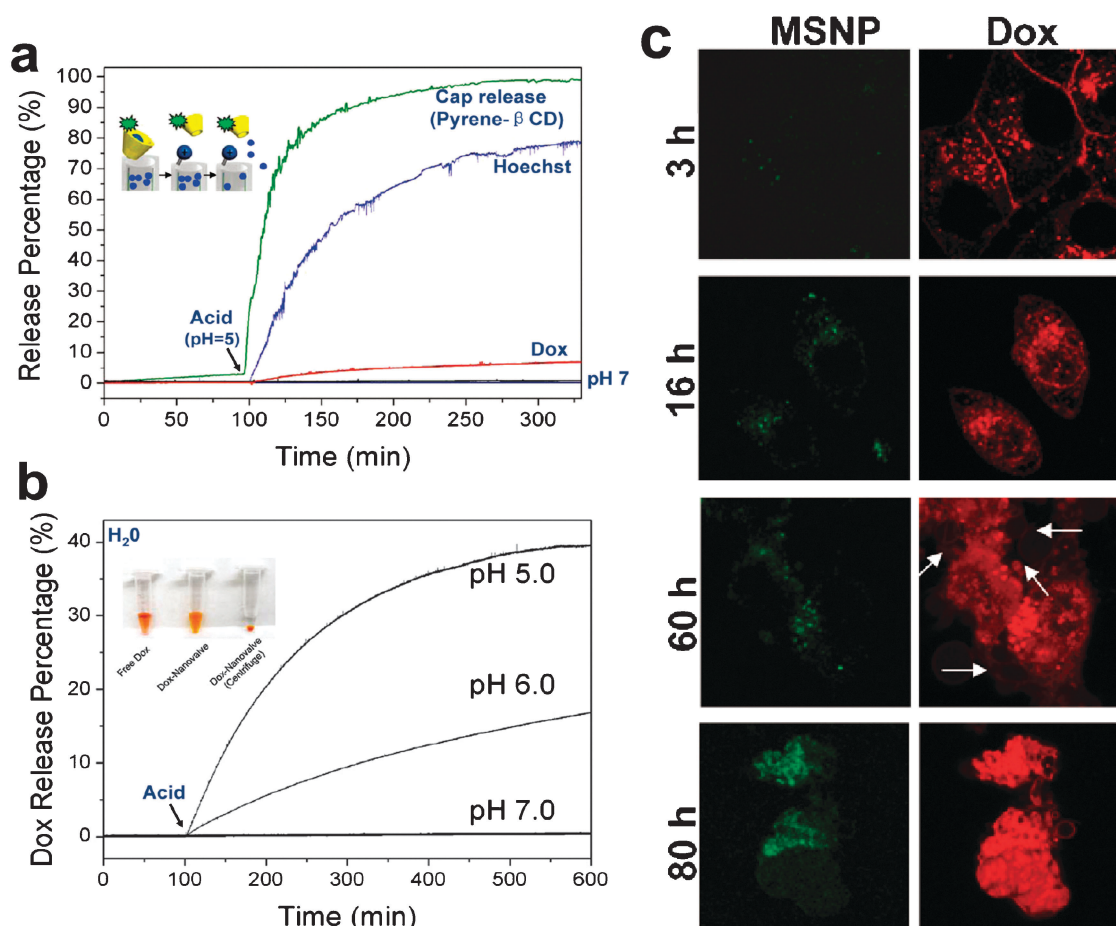


**Fig. 14** Release profiles of cargo molecules and the cyclodextrin. (a) Fluorescence intensity plots for the release of Hoechst dye, doxorubicin, and the pyrene-labeled cyclodextrin cap released from MSNP. (b) Release profiles of doxorubicin from ammonium-modified (7.5%, w/w) nanoparticles showing the faster and larger response compared to the unmodified MSNP (Fig. 14a). (c) KB-31 cancer cells effectively endocytosed the doxorubicin-loaded FITC-MSNP at 3 h. This action is followed by doxorubicin release to the nucleus, induction of cytotoxicity and appearance of apoptotic bodies by 60 h (arrow in Fig. 14c), followed by nuclear fragmentation after 80 h. (Adapted from ref. 36, Copyright 2010, American Chemical Society. Reproduced with permission.)

non-toxic in biological systems, therefore, are being highly investigated for biomedical applicability, such as the delivery of targeted drug components, therapeutic agents, and imaging agents for cancer treatment.<sup>233</sup> Recently, they reported another type of redox-responsive CDDSs which directly attaches cysteine onto the mercaptopropyl-functionalized pores of mesoporous silica nanoparticles *via* a thioether bond without caps (Structure V-a).<sup>61</sup> The stimuli-responsive release of cysteine from the system could be induced and regulated by both artificial and cell-produced natural antioxidants. More recently, Bein *et al.* synthesized a redox-driven intracellular stimuli-responsive release system, in which colloidal mesoporous silica nanoparticles with ATTO633-labeled cysteine (CysATTO633) linked to the inner particle core *via* disulfide-bridges.<sup>224</sup> Characterising the cysteine release behavior after internalization into HuH7 cells, they revealed that the release system was endocytosed by HuH7 cells without visible signs of toxicity, and endosomal escape was a bottleneck for disulfide-linkage based drug release. After photochemical rupture of the endosomes by means of a photosensitizer, the system successfully released disulfide-bound CysATTO633 into the cytoplasm, showing that the reducing milieu of the cytoplasm is sufficient

to cleave the cysteine linker. Additionally, collagen and polymer networks were also used as pore caps in disulfide-based redox-responsive CDDSs.<sup>217,234</sup>

### 4.3. Thermo-responsive and photo-irradiation-responsive CDDSs

Apart from pH and redox reactions, another popular stimuli approach is temperature. Thermo-responsive CDDSs have focused on mesoporous silica-poly (*N*-isopropyl acrylamide) composites, which have been studied thoroughly. Poly (*N*-isopropyl acrylamide) (PNIPAM), one of the most investigated temperature-sensitive polymers, can undergo a hydrophilic-hydrophobic transition at a “lower critical solution temperature” (LCST) about 32 °C.<sup>235,236</sup> Up to date, mesoporous silica-PNIPAM composites present the following two structures. One is to deposit PNIPAM polymer inside the pore of mesoporous silica particles with a larger pore size of 6–8 nm (Structure V-a), the initial mass of *N*-isopropyl acrylamide (NIPAM) monomer is less than mesoporous silica. In this system, below the LCST, the drug molecules are confined to the pores owing to (i) the swelling of the PNIPAM molecular chain that likely blocks the pores

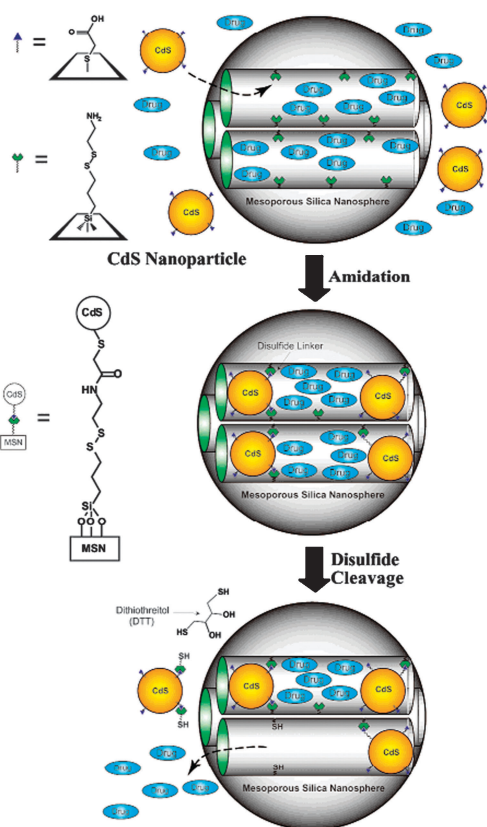


**Fig. 15** Schematic representation of the CdS nanoparticle-capped MSN-based drug/neurotransmitter delivery system. The controlled-release mechanism of the system is based on chemical reduction of the disulfide linkage between the CdS caps and the MSN hosts. (Adapted from ref. 7, Copyright 2003, American Chemical Society. Reproduced with permission.)

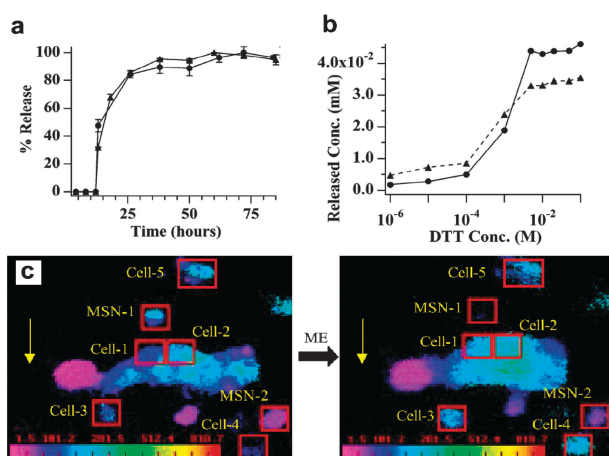


**Fig. 16** (a) The DTT-induced release profiles of Vancomycin (●) and ATP (▲) from the CdS-capped MSN system: % release over time. (b) The DTT concentration-dependent releases. Released analyte concentrations were measured with CdS-MSNs (2.3 mg) in pH 7.4 PBS buffers (0.8 mL) after 24 h of the DTT additions. (c) Effect of ATP release from CdS-capped MSNs on astrocytes. The pseudocolor images of astrocytes loaded with Fura-2 at resting level (left panel) and after the application of ME (right panel). The yellow arrows indicate the flow direction of HEPES buffer (pH 7.4). (Adapted from ref. 7, Copyright 2003, American Chemical Society. Reproduced with permission.)

to prevent drug release from the channels, and (ii) the formation of hydrogen bonds between the PNIPAM and the drug molecule (for example, IBU). Above the LCST, the polymer chains become hydrophobic and shrink within the pore network, resulting in the opening of the pores and collapse of the hydrogen bonds, driving the drug molecules to be released from the pores. Therefore, mesoporous silica–PNIPAM systems can respond to thermal stimuli from the environment. The other is to polymerize a PNIPAM shell on the exterior surface of mesoporous silica particles with a small pore size of about 2 nm (Structure III), while the initial mass of monomer is much more than that of mesoporous silica.<sup>219–221</sup> Just recently, we introduced RE luminescent phosphor into stimuli-responsive CDDSs to design luminescent rattle-type mesoporous silica microspheres with a thermo-sensitive hydrogel control switch (Fig. 17).<sup>237</sup> The multifunctional carriers exhibit a remarkable positive temperature-sensitive on–off modulation for indomethacin (IMC) release, *i.e.* rapid drug release rate at an increased temperature (“on” phase) and completely stopping at a decreased temperature (“off” phase) (Fig. 18). In addition, the emission intensity of  $\text{Gd}_2\text{O}_3:\text{Eu}^{3+}$  strongly depends on the loading and cumulative release of IMC molecules, which has potential to be used in tracking or detecting applications. The sample has the potential to serve as a  $T_1$ -MR contrast agent owing to the existence of  $\text{Gd}^{3+}$  ions in the composite. Zhu *et al.* developed a novel magnetic mesoporous silica–PNIPAM system with  $\text{Fe}_3\text{O}_4$  and  $\text{Fe}_2\text{O}_3$  particles formed *in situ* and the PNIPAM polymers are functionalized in the pore interiors (Structure V-a),<sup>226</sup> which could improve the drug-storage

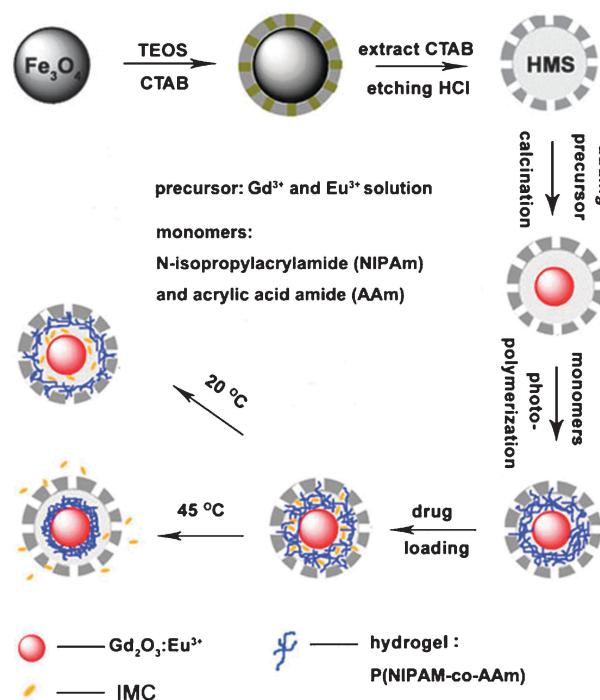


**Fig. 17** Scheme for the synthetic process for P(NIPAM-co-AAm) hydrogel modified luminescent rattle-type mesoporous silica microspheres and subsequent loading and temperature-controlled release of indomethacin (IMC) drug molecules. (Adapted from ref. 237, Copyright 2010, WILEY-VCH Verlag GmbH & Co. KGaA, Weinheim. Reproduced with permission.)

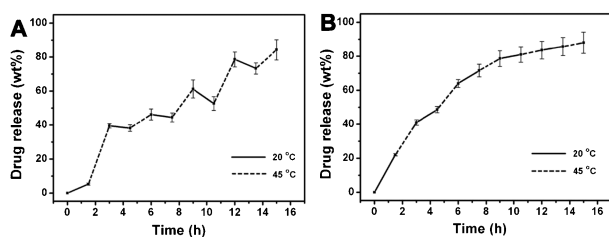


**Fig. 18** Controlled release of IMC from Gd<sub>2</sub>O<sub>3</sub>:Eu<sup>3+</sup>@P(NIPAm-co-AAm)@HMS (A) and Gd<sub>2</sub>O<sub>3</sub>:Eu<sup>3+</sup>@HMS (B) in response to temperature changes in 10 mM PBS (pH = 7.4). (Adapted from ref. 237, Copyright 2010, WILEY-VCH Verlag GmbH & Co. KGaA, Weinheim. Reproduced with permission.)

capacity of IBU from 33.5% to 71.5% contributing to the drug capture capacity of the hydrogen bond between PNIPAM and the drug molecule. Bein *et al.* and Vallet-Regí *et al.* explored a novel DNA-based thermo-responsive CDDSs,<sup>51,238</sup> in which biotin-labelled DNA double strands and DNA/magnetic nanoparticles are able to cap the pores of the mesoporous silica particles. The opening of the valve and the subsequent release of the model drug loaded in pores is achieved by DNA strands melting at the specific DNA melting temperature.

Photoirradiation-responsive CDDSs have received increased attention due to the advantages in spatial and temporal control of drug release, especially for applications in phototherapy. In the first report on photo-responsive mesoporous silica material,<sup>239</sup> Fujiwara *et al.* grafted photo-responsive coumarin onto the pore outlets of MCM-41 solids, followed by photodimerization of the coumarin by exposure to light greater than 310 nm. The photodimerization closed the pores by formation of a cyclobutane dimer spanning the pore diameter. The gate could be opened by using higher-energy irradiation at 250 nm to regenerate the coumarin monomer by photocleavage of the dimers, resulting subsequent release of the stored cholestane. Mesoporous silica functionalized with azobenzene has gained special attention owing to the photoactive responses of the hybrid. For example, Zink and co-workers prepared light-responsive mesoporous silica particles with azobenzene derivatives (tethered in the particles) as both impellers and gatekeepers (Structure V-b).<sup>211,228</sup> When excited at 413 nm, the continuous photoisomerization of the azobenzene acts as an impeller and expels the anticancer drug camptothecin out of the pores. The drug release properties can be manipulated by varying both the light intensity and the irradiation time, opening the possibilities of trapping and releasing useful molecules on demand. Notably, the light intensity of 0.1 W cm<sup>-2</sup> at 413 nm does not damage the cells. They also developed another light-responsive delivery system based on the association and light-operated dissociation of the  $\beta$ -CD (or pyrene-modified  $\beta$ -CD) rings with the azobenzene-containing stalks on the surfaces of the MCM-41 nanoparticles.<sup>210</sup> Other light-responsive CDDSs have been reported, such as light-triggered endosomal escape mechanism,<sup>240</sup> nitroveratryl moieties-modified mesoporous silica nanoparticles,<sup>223</sup> photolabile gold nanoparticles,<sup>39</sup> and spiropyran photochrom-modified mesoporous silica materials.<sup>241</sup>

#### 4.4. Biostimuli-responsive CDDSs

Most recently, novel biostimuli-responsive CDDSs to trigger the release of drug molecules involving highly desirable biomolecules under physiological conditions have become an important field. Some biomolecules, such as enzymes, glucose, antibodies, and nucleotides have been used as stimuli to unclog the mesoporous silica materials.

Enzyme-responsive controlled release is a representative example. Bein *et al.* attached avidin caps to the biotinylated colloid mesoporous silica surface.<sup>242</sup> The strong interaction of avidin–biotin complex resulted in a tight closure of the pores. Addition of the protease trypsin causes the hydrolysis of the attached protein avidin and release of the entrapped guest. Martínez-Mañez *et al.* loaded mesoporous support with [Ru(bipy)<sub>3</sub>]Cl<sub>2</sub>, and functionalized the pore outlets with different “saccharide” (Structure III).<sup>215,216</sup> The functionalized system shows “zero release” until the addition of enzyme  $\beta$ -D-galactosidase that induces the uncapping of the mesopores *via* the selective hydrolysis of the saccharides anchored on the mesoporous external surface. This is the first example of enzyme-induced in-cell delivery using capped silica mesoporous nanoparticles. In other systems, peptides, cyclodextrin and cucurbit[7]uril attached to the functionalized mesoporous silica lead to tight blocking of the nanopores.<sup>52,112,207,218,243</sup> Introduction of the corresponding enzyme, results in the release of the guest molecules from the pores.

Glucose-responsive CDDSs have also been studied. Lin *et al.* reported a glucose-responsive mesoporous silica double delivery system,<sup>244</sup> in which gluconic acid-modified insulin (G-Ins) proteins were immobilized on the exterior surface of boronic acid-functionalized mesoporous silica nanoparticles through reversible covalent bonding. G-Ins served as caps to encapsulate cyclic adenosine monophosphate (cAMP) molecules inside the mesopores of mesoporous silica. The release of both G-Ins and cAMP from mesoporous silica can be triggered by the introduction of different saccharide triggers (fructose, glucose, galactose, mannose, lactose, and maltose). Among different saccharide triggers, the release of G-Ins caps indeed showed a strong preference for fructose, followed by glucose. The high selectivity toward fructose could be explained by its high percentage of furanose form which phenylboronic acid has a strong preference for binding with, and for glucose, owing to the existence of 1:2 saccharide:boronic acid complexation for selective glucose sensing. Shi *et al.* deposited glucose oxidase enzyme (GOD) and catalase (CAT) enzyme multilayer shells onto the surface of the insulin stored mesoporous silica *via* glutaraldehyde (GA) cross-linking.<sup>63</sup> Once contacting with glucose, GOD will convert glucose into gluconic acid, which decreases the pH value of the micro-environment, then expands the volume of the enzyme multilayer shells and finally induces release of insulin from the pores. Other new classes of biostimuli-responsive CDDSs were also developed by Martínez-Mañez and others, such as (i) complementary oligonucleotide-responsive delivery of the entrapped guest in the pores of mesoporous silica with a single-stranded oligonucleotide cap,<sup>222</sup> (ii) selective release of entrapped guests by antigen-responsive mesoporous silica materials with antibodies as gatekeepers on the surface;<sup>245</sup> and



(iii) glutathione-triggered release of guest molecules from the pore of mesoporous silica CDDS equipped with cyclodextrins gatekeeper.<sup>246</sup>

## 5. Conclusion and outlook

In this review, we have highlighted some exciting research progress on mesoporous silica-based materials as sustained-release systems and stimuli-responsive controlled release systems. Among them, multifunctional mesoporous silica with luminescence and/or magnetism which integrates targeting and tracking abilities of drug molecules is currently under extensive investigation. Although these developments are encouraging and show great potential, several key challenges still need to be overcome for this controlled drug delivery system to further advance its biological and biomedical applications. First, it is crucial to design novel types of multifunctional (magnetic and luminescent) mesoporous silica composites which can load multiple drugs and offer controlled release properties. Although there are some reports on hollow mesoporous silica materials with high surface area and pore volumes which enable high drug loading and low release rate, large-scale synthesis is difficult, the methods are very limited and a functional structure is rare. Moreover, rare-earth phosphor which offers exciting opportunities for efficient luminescence functionalization still needs to be intensively investigated. Secondly, even though the intracellular delivery of several drugs in animal cells by mesoporous silica materials has been achieved, there are still many unsettled questions for future practical applications, such as biodistribution, the acute and chronic toxicities, long-term stability, circulation properties and targeting efficacy *in vivo*. Particularly, detailed biodistribution and toxicological studies of the delivery systems are necessary before they can begin to be used in humans.

Financial support from the National High Technology Research Program of China (2011AA03A407), National Basic Research Program of China (2010CB327704), the National Natural Science Foundation of China (NSFC 51172228, 21101149, 20901074, 20921002), and Research Fund for the Doctoral Program of Higher Education of China (20112304110021) and the Fundamental Research Funds for the Central Universities of China (HEUCF201210009) are greatly acknowledged.

## References

- C. T. Kresge, M. E. Leonowicz, W. J. Roth, J. C. Vartuli and J. S. Beck, *Nature*, 1992, **359**, 710–712.
- Y. Liu, W. Zhang and T. J. Pinnavaia, *J. Am. Chem. Soc.*, 2000, **122**, 8791–8792.
- Y. Liu, W. Zhang and T. J. Pinnavaia, *Angew. Chem., Int. Ed.*, 2001, **40**, 1255–1258.
- Y. Han, D. Li, L. Zhao and F. S. Xiao, *Angew. Chem., Int. Ed.*, 2003, **42**, 3633–3637.
- B. Muñoz, A. Rámila, J. Pérez-Pariente, I. Diaz and M. Vallet-Regí, *Chem. Mater.*, 2003, **15**, 500–503.
- C. Barbé, J. Bartlett, L. Kong, K. Finnie, H. Q. Lin, M. Larkin, S. Calleja, A. Bush and G. Calleja, *Adv. Mater.*, 2004, **16**, 1959–1966.
- C.-Y. Lai, B. G. Trewyn, D. M. Jeftinija, K. Jeftinija, S. Xu, S. Jeftinija and V. S.-Y. Lin, *J. Am. Chem. Soc.*, 2003, **125**, 4451–4459.
- J. Shi, Z. Hua and L. Zhang, *J. Mater. Chem.*, 2004, **14**, 795–806.
- Q. He, X. Cui, F. Cui, L. Guo and J. Shi, *Microporous Mesoporous Mater.*, 2009, **117**, 609–616.
- Q. He, J. Shi, J. Zhao, Y. Chen and F. Chen, *J. Mater. Chem.*, 2009, **19**, 6498–6503.
- Q. He, J. Shi, X. Cui, J. Zhao, Y. Chen and J. Zhou, *J. Mater. Chem.*, 2009, **19**, 3395–3403.
- M. Vallet-Regí, A. Rámila, R. P. del Real and J. Pérez-Pariente, *Chem. Mater.*, 2001, **13**, 308–311.
- R. Langer and D. A. Tirrell, *Nature*, 2004, **428**, 487–492.
- D. A. LaVan, T. McGuire and R. Langer, *Nat. Biotechnol.*, 2003, **21**, 1184–1191.
- V. P. Torchilin, *Nat. Rev. Drug Discovery*, 2005, **4**, 145–160.
- J. W. Yoo and C. H. Lee, *J. Controlled Release*, 2006, **112**, 1–14.
- M. Malmsten, *Soft Matter*, 2006, **2**, 760–769.
- M. Vallet-Regí, *Chem.–Eur. J.*, 2006, **12**, 5934–5943.
- E. Tasciotti, K. Plant, R. Bhavane, X. Liu, A. D. Leonard, K. Price, M. M. C. Cheng, P. Decuzzi, J. M. Tour, F. Robertson and M. Ferrari, *Nat. Nanotechnol.*, 2008, **3**, 151–157.
- M. Van Speybroeck, V. Barillaro, T. D. Thi, R. Mellaerts, J. Martens, J. V. Humbeeck, J. Vermant, P. Annaert, G. V. den Mooter and P. Augustijns, *J. Pharm. Sci.*, 2009, **98**, 2648–2658.
- Z. Li, J. C. Barnes, A. Bosoy, J. F. Stoddart and J. I. Zink, *Chem. Soc. Rev.*, 2012, DOI: 10.1039/C1CS15246G.
- Q. He, J. Zhang, J. Shi, Z. Zhu, L. Zhang, W. Bu, L. Guo and Y. Chen, *Biomaterials*, 2010, **31**, 1085–1092.
- I. I. Slowing, C.-W. Wu, J. L. Vivero-Escoto and V. S. Y. Lin, *Small*, 2009, **5**, 57–62.
- Y. S. Lin and C. L. Haynes, *J. Am. Chem. Soc.*, 2010, **132**, 4834–4842.
- Q. He, J. Zhang, F. Chen, L. Guo, Z. Zhu and J. Shi, *Biomaterials*, 2010, **31**, 7785–7796.
- Z. Xu, Y. Gao, S. Huang, P. A. Ma, J. Lin and J. Fang, *Dalton Trans.*, 2011, **40**, 4846–4854.
- S. Gai, P. Yang, P. a. Ma, D. Wang, C. Li, X. Li, N. Niu and J. Lin, *J. Mater. Chem.*, 2011, **21**, 16420–16426.
- Q. He, J. Shi, M. Zhu, Y. Chen and F. Chen, *Microporous Mesoporous Mater.*, 2010, **131**, 314–320.
- V. Cauda, A. Schlossbauer and T. Bein, *Microporous Mesoporous Mater.*, 2010, **132**, 60–71.
- A. Garcia, M. Colilla, I. Izquierdo-Barba and M. Vallet-Regí, *Chem. Mater.*, 2009, **21**, 4135–4145.
- Q. He, Z. Zhang, F. Gao, Y. Li and J. Shi, *Small*, 2011, **7**, 271–280.
- J. Lu, M. Liong, Z. Li, J. I. Zink and F. Tamanoi, *Small*, 2010, **6**, 1794–1805.
- S. P. Hudson, R. F. Padera, R. Langer and D. S. Kohane, *Biomaterials*, 2008, **29**, 4045–4055.
- J. S. Souris, C. H. Lee, S. H. Cheng, C. T. Chen, C. S. Yang, J. A. A. Ho, C. Y. Mou and L. W. Lo, *Biomaterials*, 2010, **31**, 5564–5574.
- Y. Zhu, T. Ikoma, N. Hanagata and S. Kaskel, *Small*, 2010, **6**, 471–478.
- H. Meng, M. Xue, T. Xia, Y.-L. Zhao, F. Tamanoi, J. F. Stoddart, J. I. Zink and A. E. Nel, *J. Am. Chem. Soc.*, 2010, **132**, 12690–12697.
- M. Liong, J. Lu, M. Kovochich, T. Xia, S. G. Ruehm, A. E. Nel, F. Tamanoi and J. I. Zink, *ACS Nano*, 2008, **2**, 889–896.
- P.-J. Chen, S.-H. Hu, C.-S. Hsiao, Y.-Y. Chen, D.-M. Liu and S.-Y. Chen, *J. Mater. Chem.*, 2011, **21**, 2535–2543.
- J. L. Vivero-Escoto, I. I. Slowing, C.-W. Wu and V. S. Y. Lin, *J. Am. Chem. Soc.*, 2009, **131**, 3462–3463.
- Y. Chen, H. Chen, M. Ma, F. Chen, L. Guo, L. Zhang and J. Shi, *J. Mater. Chem.*, 2011, **21**, 5290–5298.
- H. Wu, G. Liu, S. Zhang, J. Shi, L. Zhang, Y. Chen, F. Chen and H. Chen, *J. Mater. Chem.*, 2011, **21**, 3037–3045.
- S. Huang, P. Yang, Z. Cheng, C. Li, Y. Fan, D. Kong and J. Lin, *J. Phys. Chem. C*, 2008, **112**, 7130–7137.
- Y. Zhu, J. Shi, W. Shen, X. Dong, J. Feng, M. Ruan and Y. Li, *Angew. Chem., Int. Ed.*, 2005, **44**, 5083–5087.
- Y. Zhu, E. Kockrick, T. Ikoma, N. Hanagata and S. Kaskel, *Chem. Mater.*, 2009, **21**, 2547–2553.
- Q. Gan, X. Lu, Y. Yuan, J. Qian, H. Zhou, X. Lu, J. Shi and C. Liu, *Biomaterials*, 2011, **32**, 1932–1942.
- P. Yang, P. Yang, X. Teng, J. Lin and L. Huang, *J. Mater. Chem.*, 2011, **21**, 5505–5510.

- 47 Y. Zhu and J. Shi, *Microporous Mesoporous Mater.*, 2007, **103**, 243–249.
- 48 J. C. Doadrio, E. M. B. Sousa, I. Izquierdo-Barba, A. L. Doadrio, J. Pérez-Pariente and M. Vallet-Regí, *J. Mater. Chem.*, 2006, **16**, 462–466.
- 49 F. Balas, M. Manzano, P. Horcajada and M. Vallet-Regí, *J. Am. Chem. Soc.*, 2006, **128**, 8116–8117.
- 50 C. Liu, J. Guo, W. Yang, J. Hu, C. Wang and S. Fu, *J. Mater. Chem.*, 2009, **19**, 4764–4770.
- 51 E. Ruiz-Hernández, A. Baeza and M. Vallet-Regí, *ACS Nano*, 2011, **5**, 1259–1266.
- 52 K. Patel, S. Angelos, W. R. Dichtel, A. Coskun, Y.-W. Yang, J. I. Zink and J. F. Stoddart, *J. Am. Chem. Soc.*, 2008, **130**, 2382–2383.
- 53 R. Casasús, E. Climent, M. D. Marcos, R. Martínez-Mañez, F. Sancenón, J. Soto, P. Amorós, J. Cano and E. Ruiz, *J. Am. Chem. Soc.*, 2008, **130**, 1903–1917.
- 54 S. Angelos, N. M. Khashab, Y.-W. Yang, A. Trabolsi, H. A. Khatib, J. F. Stoddart and J. I. Zink, *J. Am. Chem. Soc.*, 2009, **131**, 12912–12914.
- 55 L. Du, S. Liao, H. A. Khatib, J. F. Stoddart and J. I. Zink, *J. Am. Chem. Soc.*, 2009, **131**, 15136–15142.
- 56 J. Liu and X. Du, *J. Mater. Chem.*, 2010, **20**, 3642–3649.
- 57 S. Angelos, E. Choi, F. Voegtle, L. De Cola and J. I. Zink, *J. Phys. Chem. C*, 2007, **111**, 6589–6592.
- 58 E. Aznar, M. Dolores Marcos, R. Martínez-Mañez, F. Sancenón, J. Soto, P. Amorós and C. Guillem, *J. Am. Chem. Soc.*, 2009, **131**, 6833–6843.
- 59 S. Huang, C. Li, P. Yang, C. Zhang, Z. Cheng, Y. Fan and J. Lin, *Eur. J. Inorg. Chem.*, 2010, 2655–2662.
- 60 M. Vallet-Regí, F. Balas, M. Colilla and M. Manzano, *Prog. Solid State Chem.*, 2008, **36**, 163–191.
- 61 R. Mortera, J. Vivero-Escoto, I. I. Slowing, E. Garrone, B. Onida and V. S. Y. Lin, *Chem. Commun.*, 2009, 3219–3221.
- 62 A. Bernardos, E. Aznar, C. Coll, R. Martínez-Mañez, J. Manuel Barat, M. Dolores Marcos, F. Sancenón, A. Benito and J. Soto, *J. Controlled Release*, 2008, **131**, 181–189.
- 63 W. Zhao, H. Zhang, Q. He, Y. Li, J. Gu, L. Li, H. Li and J. Shi, *Chem. Commun.*, 2011, **47**, 9459–9461.
- 64 P. Horcajada, A. Rámila, J. Pérez-Pariente and M. Vallet-Regí, *Microporous Mesoporous Mater.*, 2004, **68**, 105–109.
- 65 I. Izquierdo-Barba, A. Martínez, A. L. Doadrio, J. Pérez-Pariente and M. Vallet-Regí, *Eur. J. Pharm. Sci.*, 2005, **26**, 365–373.
- 66 F. Qu, G. Zhu, S. Huang, S. Li, J. Sun, D. Zhang and S. Qiu, *Microporous Mesoporous Mater.*, 2006, **92**, 1–9.
- 67 J. Andersson, J. Rosenholm, S. Areva and M. Lindén, *Chem. Mater.*, 2004, **16**, 4160–4167.
- 68 I. Izquierdo-Barba, E. Sousa, J. Carlos Doadrio, A. Luis Doadrio, J. Pérez-Pariente, A. Martínez, F. Babonneau and M. Vallet-Regí, *J. Sol-Gel Sci. Technol.*, 2009, **50**, 421–429.
- 69 P. Schmidt-Winkel, W. W. Lukens, D. Zhao, P. Yang, B. F. Chmelka and G. D. Stucky, *J. Am. Chem. Soc.*, 1999, **121**, 254–255.
- 70 S. Tang, X. Huang, X. Chen and N. Zheng, *Adv. Funct. Mater.*, 2010, **20**, 2442–2447.
- 71 S.-W. Song, K. Hidajat and S. Kawi, *Langmuir*, 2005, **21**, 9568–9575.
- 72 F. Balas, M. Manzano, M. Colilla and M. Vallet-Regí, *Acta Biomater.*, 2008, **4**, 514–522.
- 73 W. R. Zhao, H. R. Chen, Y. S. Li, L. Li, M. D. Lang and J. L. Shi, *Adv. Funct. Mater.*, 2008, **18**, 2780–2788.
- 74 W. Zhao, M. Lang, Y. Li, L. Lia and J. Shi, *J. Mater. Chem.*, 2009, **19**, 2778–2783.
- 75 Z. Feng, Y. Li, D. Niu, L. Li, W. Zhao, H. Chen, L. Li, J. Gao, M. Ruan and J. Shi, *Chem. Commun.*, 2008, 2629–2631.
- 76 Y. Zhu, J. Shi, W. Shen, H. Chen, X. Dong and M. Ruan, *Nanotechnology*, 2005, **16**, 2633–2638.
- 77 Y. Zhu, J. Shi, Y. Li, H. Chen, W. Shen and X. Dong, *Microporous Mesoporous Mater.*, 2005, **85**, 75–81.
- 78 Y. Zhu, J. Shi, H. Chen, W. Shen and X. Dong, *Microporous Mesoporous Mater.*, 2005, **84**, 218–222.
- 79 D. Niu, Z. Ma, Y. Li and J. Shi, *J. Am. Chem. Soc.*, 2010, **132**, 15144–15147.
- 80 Y. Chen, H. Chen, Deping Zeng, Y. Tian, F. Chen, J. Feng and J. Shi, *ACS Nano*, 2010, **4**, 6001–6013.
- 81 Y. Chen, H. Chen, L. Guo, Q. He, F. Chen, J. Zhou, J. Feng and J. Shi, *ACS Nano*, 2010, **4**, 529–539.
- 82 H. Wu, S. Zhang, J. Zhang, G. Liu, J. Shi, L. Zhang, X. Cui, M. Ruan, Q. He and W. Bu, *Adv. Funct. Mater.*, 2011, **21**, 1850–1862.
- 83 Y. Zhu, W. Meng, H. Gao and N. Hanagata, *J. Phys. Chem. C*, 2011, **115**, 13630–13636.
- 84 Y. Zhu, Y. Fang, L. Borchardt and S. Kaskel, *Microporous Mesoporous Mater.*, 2011, **141**, 199–206.
- 85 X.-J. Wu, Y. Jiang and D. Xu, *J. Phys. Chem. C*, 2011, **115**, 11342–11347.
- 86 Y.-J. Yang, X. Tao, Q. Hou, Y. Ma, X.-L. Chen and J.-F. Chen, *Acta Biomater.*, 2010, **6**, 3092–3100.
- 87 Y.-J. Yang, X. Tao, Q. Hou and J.-F. Chen, *Acta Biomater.*, 2009, **5**, 3488–3496.
- 88 Q. G. Xiao, X. Tao and J. F. Chen, *Ind. Eng. Chem. Res.*, 2007, **46**, 459–463.
- 89 H. M. Ding, L. Shao, R. J. Liu, Q. G. Xiao and J. F. Chen, *J. Colloid Interface Sci.*, 2005, **290**, 102–106.
- 90 T. Wang, F. Chai, Q. Fu, L. Zhang, H. Liu, L. Li, Y. Liao, Z. Su, C. Wang, B. Duan and D. Ren, *J. Mater. Chem.*, 2011, **21**, 5299–5306.
- 91 C.-C. Huang, W. Huang and C.-S. Yeh, *Biomaterials*, 2011, **32**, 556–564.
- 92 W. Zhao, J. Gu, L. Zhang, H. Chen and J. Shi, *J. Am. Chem. Soc.*, 2005, **127**, 8916–8917.
- 93 M. E. Åkerman, W. C. W. Chan, P. Laakkonen, S. N. Bhatia and E. Ruoslahti, *Proc. Natl. Acad. Sci. U. S. A.*, 2002, **99**, 12617–12621.
- 94 Y. Xu, M. Mahmood, Z. Li, E. Dervishi, S. Trigwell, V. P. Zharov, N. Ali, V. Saini, A. R. Biris, D. Lupu, D. Boldor and A. S. Biris, *Nanotechnology*, 2008, **19**, 435102.
- 95 L. Neel and C. R. Acad, *Science*, 1949, **228**, 664–666.
- 96 S. Mornet, S. Vasseur, F. Grasset and E. Duguet, *J. Mater. Chem.*, 2004, **14**, 2161–2175.
- 97 E. Ruiz-Hernández, A. Lopez-Noriega, D. Arcos, I. Izquierdo-Barba, O. Terasaki and M. Vallet-Regí, *Chem. Mater.*, 2007, **19**, 3455–3463.
- 98 J. Zhou, W. Wu, D. Caruntu, M. H. Yu, A. Martin, J. F. Chen, C. J. O'Connor and W. L. Zhou, *J. Phys. Chem. C*, 2007, **111**, 17473–17477.
- 99 L. Zhang, S. Z. Qiao, Y. G. Jin, Z. G. Chen, H. C. Gu and G. Q. Lu, *Adv. Mater.*, 2008, **20**, 805–809.
- 100 S. Gai, P. Yang, C. Li, W. Wang, Y. Dai, N. Niu and J. Lin, *Adv. Funct. Mater.*, 2010, **20**, 1166–1172.
- 101 G. H. Gao, X. H. Liu, R. R. Shi, K. C. Zhou, Y. G. Shi, R. Z. Ma, E. Takayama-Muromachi and G. Z. Qiu, *Cryst. Growth Des.*, 2010, **10**, 2888–2894.
- 102 T. Hyeon, S. S. Lee, J. Park, Y. Chung and H. B. Na, *J. Am. Chem. Soc.*, 2001, **123**, 12798–12801.
- 103 N. R. Jana, Y. Chen and X. Peng, *Chem. Mater.*, 2004, **16**, 3931–3935.
- 104 J. Park, K. An, Y. Hwang, J.-G. Park, H.-J. Noh, J.-Y. Kim, J.-H. Park, N.-M. Hwang and T. Hyeon, *Nat. Mater.*, 2004, **3**, 891–895.
- 105 S. Sun and H. Zeng, *J. Am. Chem. Soc.*, 2002, **124**, 8204–8205.
- 106 C.-C. Huang, C.-Y. Tsai, H.-S. Sheu, K.-Y. Chuang, C.-H. Su, U. S. Jeng, F.-Y. Cheng, C.-H. Su, H.-Y. Lei and C.-S. Yeh, *ACS Nano*, 2011, **5**, 3905–3916.
- 107 Y. H. Deng, D. W. Qi, C. H. Deng, X. M. Zhang and D. Y. Zhao, *J. Am. Chem. Soc.*, 2008, **130**, 28–29.
- 108 X. Li, J. Zhang and H. Gu, *Langmuir*, 2011, **27**, 6099–6106.
- 109 L. Zhao, Y. Zhao and Y. Han, *Langmuir*, 2010, **26**, 11784–11789.
- 110 J. Zhang, X. Li, J. M. Rosenholm and H.-C. Gu, *J. Colloid Interface Sci.*, 2011, **361**, 16–24.
- 111 J. Kim, H. S. Kim, N. Lee, T. Kim, H. Kim, T. Yu, I. C. Song, W. K. Moon and T. Hyeon, *Angew. Chem., Int. Ed.*, 2008, **47**, 8438–8441.
- 112 J. Liu, X. Du and X. Zhang, *Chem.–Eur. J.*, 2011, **17**, 810–815.
- 113 J. Lian, X. Duan, J. Ma, P. Peng, T. Kim and W. Zheng, *ACS Nano*, 2009, **3**, 3749–3761.
- 114 S. Huang, Y. Fan, Z. Cheng, D. Kong, P. Yang, Z. Quan, C. Zhang and J. Lin, *J. Phys. Chem. C*, 2009, **113**, 1775–1784.
- 115 H. H. P. Yiu, H.-j. Niu, E. Biermans, G. van Tendeloo and M. J. Rosseinsky, *Adv. Funct. Mater.*, 2010, **20**, 1599–1609.
- 116 Y. Zhu, S. Kaskel, J. Shi, T. Wage and K.-H. V. Pée, *Chem. Mater.*, 2007, **19**, 6408–6413.

- 117 F. M. Martín-Saavedra, E. Ruiz-Hernández, A. Boré, D. Arcos, M. Vallet-Regí and N. Vilaboa, *Acta Biomater.*, 2010, **6**, 4522–4531.
- 118 L. Zhang, S. Z. Qiao, L. Cheng, Z. Yan and G. Q. Lu, *Nanotechnology*, 2008, **19**, 435608–435615.
- 119 Y. Zhu, Y. Fang and S. Kaskel, *J. Phys. Chem. C*, 2010, **114**, 16382–16388.
- 120 S. Giri, B. G. Trewyn, M. P. Stellmaker and V. S. Y. Lin, *Angew. Chem., Int. Ed.*, 2005, **44**, 5038–5044.
- 121 N. Insin, J. B. Tracy, H. Lee, J. P. Zimmer, R. M. Westervelt and M. G. Bawendi, *ACS Nano*, 2008, **2**, 197–202.
- 122 T. R. Sathe, A. Agrawal and S. M. Nie, *Anal. Chem.*, 2006, **78**, 5627.
- 123 F. Wang, W. B. Tan, Y. Zhang, X. Fan and M. Wang, *Nanotechnology*, 2006, **17**, R1.
- 124 L. Z. Wang, J. Y. Lei and J. L. Zhang, *Chem. Commun.*, 2009, (16), 2195–2197.
- 125 J. Lei, L. Wang and J. Zhang, *ACS Nano*, 2011, **5**, 3447–3455.
- 126 L.-S. Wang, L.-C. Wu, S.-Y. Lu, Li-Ling Chang, I.-T. Teng, C.-M. Yang and J.-a. A. Ho, *ACS Nano*, 2010, **4**, 4371–4379.
- 127 J. Lu, M. Liong, J. I. Zink and F. Tamanoi, *Small*, 2007, **8**, 1341–1346.
- 128 Y.-S. Lin, C.-P. Tsai, H.-Y. Huang, C.-T. Kuo, Y. Hung, D.-M. Huang, Y.-C. Chen and C.-Y. Mou, *Chem. Mater.*, 2005, **17**, 4570–4573.
- 129 J. E. Lee, N. Lee, H. Kim, J. Kim, S. H. Choi, J. H. Kim, T. Kim, I. C. Song, S. P. Park, W. K. Moon and T. Hyeon, *J. Am. Chem. Soc.*, 2010, **132**, 552–557.
- 130 T.-T. Wang, F. Chai, C.-G. Wang, L. Li, H.-Y. Liu, L.-Y. Zhang, Z.-M. Su and Y. Liao, *J. Colloid Interface Sci.*, 2011, **358**, 109–115.
- 131 T. Wang, L. Zhang, Z. Su, C. Wang, Y. Liao and Q. Fu, *ACS Appl. Mater. Interfaces*, 2011, **3**, 2479–2486.
- 132 C.-P. Tsai, C.-Y. Chen, Y. Hung, F.-H. Chang and C.-Y. Mou, *J. Mater. Chem.*, 2009, **19**, 5737–5743.
- 133 F. Wang, X. Chen, Z. Zhao, S. Tang, X. Huang, C. Lin, C. Cai and N. Zheng, *J. Mater. Chem.*, 2011, **21**, 11244–11252.
- 134 R. Zhang, C. Wu, L. Tong, B. Tang and Q.-H. Xu, *Langmuir*, 2009, **25**, 10153–10158.
- 135 M. Bruchez, M. Moronne, P. Gin, S. Weiss and A. P. Alivisatos, *Science*, 1998, **281**, 2013–2016.
- 136 W. C. W. Chan and S. Nie, *Science*, 1998, **281**, 2016–2018.
- 137 N. N. Mamedova, N. A. Kotov, A. L. Rogach and J. Studer, *Nano Lett.*, 2001, **1**, 281–186.
- 138 X. Michalet, F. F. Pinaud, L. A. Bentolila, J. M. Tsay, S. Doose, J. J. Li, G. Sundaresan, A. M. Wu, S. S. Gambhir and S. Weiss, *Science*, 2005, **307**, 538–544.
- 139 S. T. Selvan, T. T. Tan and J. Y. Ying, *Adv. Mater.*, 2005, **17**, 1620–1625.
- 140 L. Spanhel, M. Haase, H. Weller and A. Henglein, *J. Am. Chem. Soc.*, 1987, **109**, 5649–5655.
- 141 X. Peng, M. C. Schlamp, A. V. Kadavanich and A. P. Alivisatos, *J. Am. Chem. Soc.*, 1997, **119**, 7019–7029.
- 142 L. Manna, E. C. Scher and A. P. Alivisatos, *J. Am. Chem. Soc.*, 2000, **122**, 12700–12706.
- 143 C. B. Murray, D. J. Norris and M. G. Bawendi, *J. Am. Chem. Soc.*, 1993, **115**, 8706–8715.
- 144 X. Peng, J. Wickham and A. P. Alivisatos, *J. Am. Chem. Soc.*, 1998, **120**, 5343–5344.
- 145 Z. A. Peng and X. G. Peng, *J. Am. Chem. Soc.*, 2002, **124**, 3343–3353.
- 146 A. R. Clapp, E. R. Goldman and H. Mattoussi, *Nat. Protoc.*, 2006, **1**, 1258–1266.
- 147 Z. A. Peng and X. G. Peng, *J. Am. Chem. Soc.*, 2001, **123**, 183–184.
- 148 D. V. Talapin, A. L. Rogach, A. Kornowski, M. Haase and H. Weller, *Nano Lett.*, 2001, **1**, 207–211.
- 149 J. Kim, J. E. Lee, J. Lee, J. H. Yu, B. C. Kim, K. An, Y. Hwang, C.-H. Shin, J.-G. Park, J. Kim and T. Hyeon, *J. Am. Chem. Soc.*, 2006, **128**, 688–689.
- 150 X. Hu, P. Zrazhevskiy and X. Gao, *Ann. Biomed. Eng.*, 2009, **37**, 1960–1966.
- 151 J. Liu, S. B. Hartono, Y. G. Jin, Z. Li, G. Q. Lu and S. Z. Qiao, *J. Mater. Chem.*, 2010, **20**, 4595–4601.
- 152 Y. Chen, H. Chen, S. Zhang, F. Chen, L. Zhang, J. Zhang, M. Zhu, H. Wu, L. Guo, J. Feng and J. Shi, *Adv. Funct. Mater.*, 2011, **21**, 270–278.
- 153 S. T. Selvan, P. K. Patra, C. Y. Ang and J. Y. Ying, *Angew. Chem., Int. Ed.*, 2007, **46**, 2448–2452.
- 154 F. Chen and D. Gerion, *Nano Lett.*, 2004, **4**, 1827–1832.
- 155 J. Pan, D. Wan and J. Gong, *Chem. Commun.*, 2011, **47**, 3442–3444.
- 156 O. Barbier, G. Jacquillet, M. Tauc, M. Cougnon and P. Poujeol, *Nephron Physiol.*, 2005, **99**, 105–110.
- 157 R. S. H. Yang, L. W. Chang, J. P. Wu, M. H. Tsai, H. J. Wang, Y. C. Kuo, T. K. Yeh, C. S. Yang and P. Lin, *Environ. Health Perspect.*, 2007, **115**, 1339–1343.
- 158 H. C. Fischer, L. Liu, K. S. Pang and W. C. W. Chan, *Adv. Funct. Mater.*, 2006, **16**, 1299–1305.
- 159 M. Nickkova, D. Dosev, S. J. Gee, B. D. Hammock and I. M. Kennedy, *Anal. Chem.*, 2005, **77**, 6864–6873.
- 160 E. M. Goldys, K. D. Tomsia, S. Jinjun, D. Dosev, I. M. Kennedy, S. Yatsunenko and M. Godlewski, *J. Am. Chem. Soc.*, 2006, **128**, 14498–14505.
- 161 W. O. Gordon, J. A. Carter and B. M. Tissue, *J. Lumin.*, 2004, **108**, 339–342.
- 162 S. Gai, P. Yang, D. Wang, C. Li, N. Niu, F. He and X. Li, *CrystEngComm*, 2011, **13**, 5480–5487.
- 163 P. Yang, Z. Quan, C. Li, H. Lian, S. Huang and J. Lin, *Microporous Mesoporous Mater.*, 2008, **116**, 524–531.
- 164 Z. Xu, P. Ma, C. Li, Z. Hou, X. Zhai, S. Huang and J. Lin, *Biomaterials*, 2011, **32**, 4161–4173.
- 165 C. Zhang, C. Li, C. Peng, R. Chai, S. Huang, D. Yang, Z. Cheng and J. Lin, *Chem.–Eur. J.*, 2010, **16**, 5672–5680.
- 166 Z. Xu, Y. Cao, C. Li, P. Ma, X. Zhai, S. Huang, X. Kang, M. Shang, D. Yang, Y. Daiab and J. Lin, *J. Mater. Chem.*, 2011, **21**, 3686–3694.
- 167 Y. Dai, C. Zhang, Z. Cheng, P. Ma, C. Li, X. Kang, D. Yang and J. Lin, *Biomaterials*, 2012, **33**, 2583–2592.
- 168 P. Yang, Z. Quan, L. Lu, S. Huang and J. Lin, *Biomaterials*, 2008, **29**, 692–702.
- 169 P. Yan, S. Huang, D. Kong, J. Lin and H. Fu, *Inorg. Chem.*, 2007, **46**, 3203–3211.
- 170 P. Yang, Z. Quan, L. Lu, S. Huang, J. Lin and H. Fu, *Nanotechnology*, 2007, **18**, 235703.
- 171 G. Blasse and B. C. Grabmaier, *Luminescent Materials*, Springer-Verlag, Berlin, Heidelberg, 1994, ch. 4.
- 172 S. Gai, P. Yang, J. Hao, W. Wang, N. Niu, F. He, D. Wang and J. Lin, *Microporous Mesoporous Mater.*, 2010, **131**, 128–135.
- 173 D. Kong, P. Yang, Z. Wang, P. Chai, S. Huang, H. Lian and J. Lin, *J. Nanomater.*, 2008, 1–7.
- 174 D. K. Chatterjee, A. J. Rufaihah and Y. Zhang, *Biomaterials*, 2008, **29**, 937–943.
- 175 H. Hu, M. X. Yu, F. Y. Li, Z. G. Chen, X. Gao, L. Q. Xiong and C. H. Huang, *Chem. Mater.*, 2008, **20**, 7003–7009.
- 176 R. Naccache, F. Vetrone, V. Mahalingam, L. A. Cuccia and J. A. Capobianco, *Chem. Mater.*, 2009, **21**, 717–723.
- 177 M. Y. Xie, X. N. Peng, X. F. Fu, J. J. Zhang, G. L. Li and X. F. Yu, *Scr. Mater.*, 2009, **60**, 190–193.
- 178 A. C. Tropper, J. N. Carter, R. D. T. Lauder, D. C. Hanna, S. T. Davey and D. J. Szebesta, *J. Opt. Soc. Am. B*, 1994, **11**, 886–893.
- 179 M. X. Yu, F. Y. Li, Z. G. Chen, H. Hu, C. Zhan, H. Yang and C. H. Huang, *Anal. Chem.*, 2009, **81**, 930–935.
- 180 R. A. Jalil and Y. Zhang, *Biomaterials*, 2008, **29**, 4122–4128.
- 181 C. T. Xu, N. Svensson, J. Axelsson, P. Svenmarker, G. Somesfalean, G. Y. Chen, H. J. Liang, H. C. Liu, Z. G. Zhang and S. Andersson–Engels, *Appl. Phys. Lett.*, 2008, **93**, 171103.
- 182 L. Y. Wang, R. X. Yan, Z. Y. Hao, L. Wang, J. H. Zeng, X. W. J. Bao, Q. Peng and Y. D. Li, *Angew. Chem., Int. Ed.*, 2005, **44**, 6054–6057.
- 183 S. Heer, K. Kompe, H. U. Gudel and M. Haase, *Adv. Mater.*, 2005, **17**, 2119–2123.
- 184 V. V. D. Rijke, H. Zijlmans, S. Li, T. Vail, A. K. Raap, R. S. Niedbala and H. J. Tanke, *Nat. Biotechnol.*, 2001, **19**, 273–276.
- 185 R. J. Palmer, J. L. Butenhoff and J. B. Stevens, *Environ. Res.*, 1987, **44**, 142–156.
- 186 D. R. Larson, W. R. Zipfel, R. M. Williams, S. W. Clark, M. P. Bruchez, F. W. Wize and W. W. Webb, *Science*, 2003, **300**, 1434–1436.
- 187 X. Kang, Z. Cheng, C. Li, D. Yang, M. Shang, P. a. Ma, G. Li, N. Liu and J. Lin, *J. Phys. Chem. C*, 2011, **115**, 15801–15811.



- 188 Z. Xu, C. Li, P. a. Ma, Z. Hou, D. Yang, X. Kang and J. Lin, *Nanoscale*, 2011, **3**, 661–667.
- 189 Y. Wei, F. Q. Lu, X. R. Zhang and D. P. Chen, *Chem. Mater.*, 2006, **18**, 5733–5737.
- 190 C. H. Liu and D. Chen, *J. Mater. Chem.*, 2007, **17**, 3875–3880.
- 191 G. F. Wang, Q. Peng and Y. D. Li, *J. Am. Chem. Soc.*, 2009, **131**, 14200–14201.
- 192 L. Y. Wang and Y. D. Li, *Chem. Commun.*, 2006, 2557–2559.
- 193 P. Li, Q. Peng and Y. D. Li, *Adv. Mater.*, 2009, **21**, 1945–1948.
- 194 C. H. Liu, H. Wang, X. R. Zhang and D. Chen, *J. Mater. Chem.*, 2009, **19**, 489–496.
- 195 Z. Q. Li, Y. Zhang and S. Jiang, *Adv. Mater.*, 2008, **20**, 4765–4769.
- 196 Z. Hou, C. Li, P. Ma, G. Li, Z. Cheng, C. Peng, D. Yang, P. Yang and J. Lin, *Adv. Funct. Mater.*, 2011, **21**, 2356–2365.
- 197 Y. G. Sun and Y. N. Xia, *Science*, 2002, **298**, 2176–2179.
- 198 Y. L. Wang and Y. N. Xia, *Nano Lett.*, 2004, **4**, 2047–2050.
- 199 Y. Lu, Y. B. Yin, T. Mayers and Y. Xia, *Nano Lett.*, 2002, **2**, 183–186.
- 200 P. Yang, Z. Quan, Z. Hou, C. Li, X. Kang, Z. Cheng and J. Lin, *Biomaterials*, 2009, **30**, 4786–4795.
- 201 Y. Zhu, S. Kaskel, T. Ikoma and N. Hanagata, *Microporous Mesoporous Mater.*, 2009, **123**, 107–112.
- 202 G. Ferey, C. Mellot-Draznieks, C. Serre, F. Millange, J. Dutour, S. Surble and I. Margiolaki, *Science*, 2005, **309**, 2040–2042.
- 203 T. Azaus, C. Tournq-Pqteilh, F. Aussenac, N. Baccile, C. Coelho, J. M. Devoisselle and F. Babonneau, *Chem. Mater.*, 2006, **18**, 6382–6390.
- 204 J. Fan, C. Yu, F. Gao, J. Lei, B. Tian, L. Wang, Q. Luo, B. Tu, W. Zhou and D. Zhao, *Angew. Chem., Int. Ed.*, 2003, **42**, 3146–3150.
- 205 F. Muharnmad, M. Guo, W. Qi, F. Sun, A. Wang, Y. Guo and G. Zhu, *J. Am. Chem. Soc.*, 2011, **133**, 8778–8781.
- 206 C. Park, K. Oh, S. C. Lee and C. Kim, *Angew. Chem., Int. Ed.*, 2007, **46**, 1455–1457.
- 207 C. Park, H. Kim, S. Kim and C. Kim, *J. Am. Chem. Soc.*, 2009, **131**, 16614–16615.
- 208 W. Guo, J. Wang, S.-J. Lee, F. Dong, S. S. Park and C.-S. Ha, *Chem.–Eur. J.*, 2010, **16**, 8641–8646.
- 209 Y.-L. Zhao, Z. Li, S. Kabehie, Y. Y. Botros, J. F. Stoddart and J. I. Zink, *J. Am. Chem. Soc.*, 2010, **132**, 13016–13025.
- 210 D. P. Ferris, Y.-L. Zhao, N. M. Khashab, H. A. Khatib, J. F. Stoddart and J. I. Zink, *J. Am. Chem. Soc.*, 2009, **131**, 1686–1688.
- 211 S. Angelos, Y.-W. Yang, N. M. Khashab, J. F. Stoddart and J. I. Zink, *J. Am. Chem. Soc.*, 2009, **131**, 11344–11346.
- 212 N. M. Khashab, M. E. Belowich, A. Trabolsi, D. C. Friedman, C. Valente, Y. Lau, H. A. Khatib, J. I. Zink and J. F. Stoddart, *Chem. Commun.*, 2009, 5371–5373.
- 213 T. D. Nguyen, K. C.-F. Leung, M. Liong, C. D. Pentecost, J. F. Stoddart and J. I. Zink, *Org. Lett.*, 2006, **8**, 3363–3366.
- 214 E. Aznar, C. Coll, M. Dolores Marcos, R. Martínez-Mañez, F. Sancenón, J. Soto, P. Amorós, J. Cano and E. Ruiz, *Chem.–Eur. J.*, 2009, **15**, 6877–6888.
- 215 A. Bernardos, E. Aznar, M. Dolores Marcos, R. Martínez-Mañez, F. Sancenón, J. Soto, J. Manuel Barat and P. Amorós, *Angew. Chem., Int. Ed.*, 2009, **48**, 5884–5887.
- 216 A. Bernardos, L. Mondragón, E. Aznar, M. D. Marcos, R. Martínez-Mañez, F. Sancenón, J. Soto, J. M. Barat, E. Pérez-Payá, C. Guillem and P. Amorós, *ACS Nano*, 2010, **4**, 6353–6368.
- 217 R. Liu, X. Zhao, T. Wu and P. Feng, *J. Am. Chem. Soc.*, 2008, **130**, 14418–14419.
- 218 C. Coll, L. Mondragón, R. Martínez-Mañez, F. Sancenón, M. Dolores Marcos, J. Soto, P. Amorós and E. Pérez-Payá, *Angew. Chem., Int. Ed.*, 2011, **50**, 2138–2140.
- 219 C.-Y. Hong, X. Li and C.-Y. Pan, *J. Phys. Chem. C*, 2008, **112**, 15320–15324.
- 220 B. Chang, X. Sha, J. Guo, Y. Jiao, C. Wang and W. Yang, *J. Mater. Chem.*, 2011, **21**, 9239–9247.
- 221 P.-W. Chung, R. Kumar, M. Pruski and V. S. Y. Lin, *Adv. Funct. Mater.*, 2008, **18**, 1390–1398.
- 222 E. Climent, R. Martínez-Mañez, F. Sancenón, M. D. Marcos, J. Soto, A. Maquieira and P. Amorós, *Angew. Chem., Int. Ed.*, 2010, **49**, 7281–7283.
- 223 N. Z. Knezevic, B. G. Trewyn and V. S. Y. Lin, *Chem.–Eur. J.*, 2011, **17**, 3338–3342.
- 224 A. M. Sauer, A. Schlossbauer, N. Ruthardt, V. Cauda, T. Bein and C. Bräuchle, *Nano Lett.*, 2010, **10**, 3684–3691.
- 225 S. Zhu, Z. Zhou, D. Zhang, C. Jin and Z. Li, *Microporous Mesoporous Mater.*, 2007, **106**, 56–61.
- 226 S. Zhu, Z. Zhou and D. Zhang, *ChemPhysChem*, 2007, **8**, 2478–2483.
- 227 B.-S. Tian and C. Yang, *J. Phys. Chem. C*, 2009, **113**, 4925–4931.
- 228 J. Lu, E. Choi, F. Tamanoi and J. I. Zink, *Small*, 2008, **4**, 421–426.
- 229 M. Z. I. Khan, N. Prebeg and N. Kurjaković, *J. Controlled Release*, 1999, **58**, 215–222.
- 230 L. E. Gerweck, *Semin. Radiat. Oncol.*, 1998, **8**, 176–182.
- 231 J. L. Wike-Hooley, J. Haveman and H. S. Reinhold, *Radiother. Oncol.*, 1984, **2**, 343–366.
- 232 J. A. Gruenhagen, C.-Y. Lai, D. R. Radu, V. S. Y. Lin and E. S. Yeung, *Appl. Spectrosc.*, 2005, **59**, 424–431.
- 233 J. Khandare, M. Calderón, N. M. Dagiaa and R. Haag, *Chem. Soc. Rev.*, 2011, DOI: 10.1039/C1CS15242D.
- 234 Z. Luo, K. Cai, Y. Hu, L. Zhao, P. Liu, L. Duan and W. Yang, *Angew. Chem., Int. Ed.*, 2011, **50**, 640–643.
- 235 M. Heskins and J. E. Guillet, *J. Macromol. Sci. Chem.*, 1968, **A2**, 1441–1455.
- 236 H. G. Schild, *Prog. Polym. Sci.*, 1992, **17**, 163–249.
- 237 X. Kang, Z. Cheng, D. Yang, P. Ma, M. Shang, C. Peng, Y. Dai and J. Lin, *Adv. Funct. Mater.*, 2012, DOI: 10.1002/adfm.201102746.
- 238 A. Schlossbauer, S. Warncke, P. M. E. Gramlich, J. Kecht, A. Manetto, T. Carell and T. Bein, *Angew. Chem., Int. Ed.*, 2010, **49**, 4734–4737.
- 239 N. K. Mal, M. Fujiwara and Y. Tanaka, *Nature*, 2003, **421**, 350–353.
- 240 S. Febvay, D. M. Marini, A. M. Belcher and D. E. Clapham, *Nano Lett.*, 2010, **10**, 2211–2219.
- 241 E. Aznar, R. Casasús, B. García-Acosta, M. D. Marcos, R. Martínez-Mañez, F. Sancenón, J. Soto and P. Amorós, *Adv. Mater.*, 2007, **19**, 2228–2231.
- 242 A. Schlossbauer, J. Kecht and T. Bein, *Angew. Chem., Int. Ed.*, 2009, **48**, 3092–3095.
- 243 P. D. Thornton and A. Heise, *J. Am. Chem. Soc.*, 2010, **132**, 2024–2028.
- 244 Y. Zhao, B. G. Trewyn, I. I. Slowing and V. S.-Y. Lin, *J. Am. Chem. Soc.*, 2009, **131**, 8398–8400.
- 245 E. Climent, A. Bernardos, R. Martínez-Mañez, A. Maquieira, M. Dolores Marcos, N. Pastor-Navarro, R. Puchades, F. Sancenón, J. Soto and P. Amorós, *J. Am. Chem. Soc.*, 2009, **131**, 14075–14080.
- 246 H. Kim, S. Kim, C. Park, H. Lee, H. J. Park and C. Kim, *Adv. Mater.*, 2010, **22**, 4280–4283.